Optimized well positioning for down-gradient capture of infiltrated water

The impact of groundwater flow and storage conditions

MSc thesis of the research master program Earth Surface and Water in the Hydrology track, Faculty of Geosciences, Utrecht University

Jens van Griensven

6148603

Utrecht University supervisor:

dr. N. Hartog (UU)

KWR supervisor:

L. P. Brokx (KWR)

Number of ECTS: 30
7 July 2023

Utrecht University

KWR

Abstract

The recovery of single-well aquifer storage and recovery (ASR) systems is negatively impacted by background flow. Here, the benefits and risks of using a down-gradient abstraction well in an aquifer storage transfer and recovery (ASTR) system were studied. A one-layered model was constructed using MODFLOW 6, to evaluate the effect of ambient flow, dispersion, injection volume and uncertainties in magnitude and angle of the flow velocity on the RE and optimized down-gradient well position. Numerical modelling showed that the numerical optimized well distance closely relates to the analytical calculated displacement distance for longitudinal dispersivities ≤ 0.5 m. At these dispersivities, ASTR systems at optimized well distances, with ambient flow > 0 m/y result in higher RE's compared to ASR systems up to 60% of the total injected water volume. Smaller injection volumes with smaller resulting hydraulic radii showed high sensitivity to edge effects decreasing both the optimized well distance and corresponding optimized RE. Uncertainties in angle and magnitude of the groundwater flow decrease the effectivity of the optimized well positioning and with that also the RE drops. ASTR systems are potentially powerful systems to increase RE in regions with ambient flow. Their success is, however, highly dependent on the accurate determination of subsurface parameters, such as direction and magnitude of ambient flow.

Keywords: ASR, ASTR, ambient flow, well distance, recovery efficiency.

Index

1. Introduction

1.1 Background

Currently, the global freshwater use is approximately 4,600 km^3 and with the predicted increase in population to over 9.4 billion in the year 2050, lifestyle changes and increased industrialization the water stress increases globally with 20-30%, affecting the food security in both arid and humid regions (Boretti & Rosa, 2019; Hajek & Knapp, 2022; Scanlon et al., 2023). On top of that, climate change increases the stress on freshwater availability (Dettinger et al., 2015; Intergovernmental Panel on Climate, 2022; Liu et al., 2023; Rasmussen et al., 2013; Zuurbier & Stuyfzand, 2017). Climate change can increase the seasonal variability in water availability, exposing society to temporal water shortages, even in regions with a yearly positive water balance (Intergovernmental Panel on Climate, 2022). Freshwater storage is an effective method to bridge this temporal gap between wet and dry seasons and create access to freshwater throughout the year.

Typical surface freshwater storage methods are reservoirs and silos. These solutions often have disadvantages like loss due to evaporation, high building cost, requirement of large surface area, vulnerability to contamination, biodiversity loss and accumulation of sediment (Bouwer, 2002; Page et al., 2018). Aquifer storage and recovery (ASR) is an alternative to surface storage. This subsurface storage in aquifers offers a low-cost solution with high storage capacity in aquifers, protection from evaporation and requirement of little space at the surface (Ringleb et al., 2016; Zuurbier et al., 2013; Zuurbier et al., 2017).

ASR techniques are focusing on injecting and recovering high quality water in aquifers with lower quality, e.g., saline, or brackish aquifers. The water is directly injected into the subsurface without creating artificial subsurface basins. Generally, ASR systems are outfitted with a single pump connected to a freshwater supply. In times of abundance, surpluses of freshwater can be pumped into aquifers, where it remains during a storage period (Ward et al., 2009). When water demand increases and surface resources are not sufficient, the stored injection volume can be extracted. Depending on the quality of injected water, the extracted water is suitable for urban, irrigational or industrial purposes (Zuurbier et al., 2014). Due to their versatile application, ASR systems are developed abundantly worldwide (Bloetscher et al., 2014; Rinck-Pfeiffer et al., 2000). In the Netherlands, ASR is used for storage of rainwater, drinking water and surface runoff from freshwater bodies (PWN, 2022; Zuurbier et al., 2014).

1.2 Problem statement

An important factor that affects the performance in ASR systems is the ambient groundwater flow (Zuurbier et al., 2013). The ambient flow is the movement of water through a porous medium due to a hydraulic gradient. During the storage period, the injected freshwater volume is not isolated and stationary. Mechanical dispersion and molecular diffusion can result in mixing of injected freshwater and ambient groundwater. Furthermore, the injected water volume may move and deform due to ambient groundwater flow (Ceric & Haitjema, 2005). Instead of a circular water column around the well, the injected water may develop into an ellipsoidal shape during injection, which is laterally moving downstream during storage. After storage the extraction starts. Now, the upstream ambient water approaches the well faster than the injected water (Figure 1). The volume of injected water that is not recovered during extraction is lost and therefore impacts the performance (Ward et al., 2009).

Using an Aquifer Storage, Transfer and Recovery (ASTR) setup with an extraction well located downstream from the injection well, the injected water displaced by ambient flow may be better recoverable (Figure 2). In regions with high ambient flow, where performance of ASR systems drastically decreases (Bear & Jacobs, 1965), this ASTR approach may serve as a valuable alternative to ASR (Miotliński et al., 2014; Zuurbier et al., 2014). However, this ASTR approach brings more uncertainty in the performance and design than ASR. The downstream extraction well location needs to be determined based on subsurface parameters, which are often not extensively available. The limited knowledge on flow conditions gives rise to uncertainties om the angle and magnitude of ambient flow. As a result, the

injection and extraction well may not be placed at the optimal locations with respect to each other, which may decrease performance of the ASTR solution. Nevertheless, optimized placement of the downstream extraction well, based on well-established parameters may be a step towards high recovery in ASTR applications.

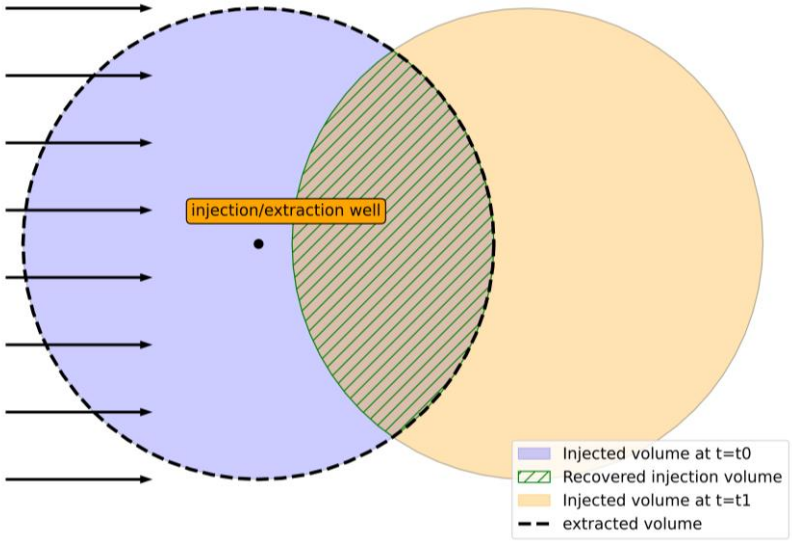

Figure 1. ASR system in a flow field based on capture zone Ceric and Haitjema (2005), with intial injected volume (blue), transferred injected volume and extracted volume (dotted line).

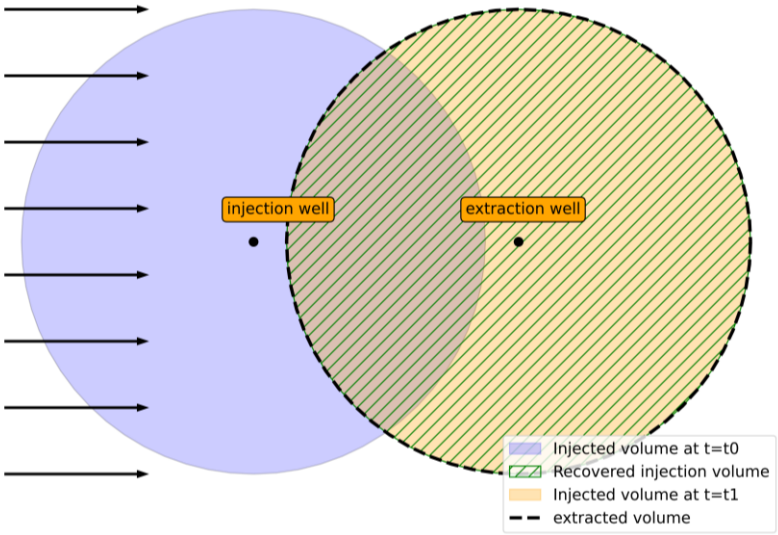

Figure 2. ASTR system with a separated injection (left) and extraction well (right). After injection, the volume moves towards the extraction well. Freshwater injection finalized at t=t0, extraction begins at end of storage period t=t1.

1.3 Aim and approach

ASR and ASTR systems are both vulnerable to subsurface processes during the injection, storage and extraction phase. The aim of this study was to determine the relative performance of ASR and ASTR systems under different ambient flow, dispersion and injected freshwater volume conditions. Based on the following sub questions and with use of a numerical MODFLOW 6 model, the research objective was evaluated.

- What is the optimized position for a downstream capture well in an ASTR system given the ambient flow and abstraction and infiltration volumes?

Before assessing relative performance of ASR to ASTR, the performance of the optimized ASTR system must be identified. This was done by numerically determining the most optimized location for the extraction well, the performance of the ASTR system was calculated for a range of well distances. The optimized location was evaluated in several scenarios over a range of different ambient flow values.

- How does the performance of the ASTR system change depending on ambient flow conditions with respect to an ASR system?

When ambient flow is present in an aquifer, injected freshwater volumes can move (Miotliński et al., 2014; Zuurbier et al., 2014). The goal was to evaluate the added value of optimized ASTR systems over ASR systems. Both relative and absolute gains in RE were assessed to study potential of ASTR solutions under changing ambient flow conditions.

- How does dispersion affect the performance of the ASR and ASTR systems?

Mixing of ambient groundwater with injected freshwater occurs at the edges of the injected volume. Due to dispersion the injected water volume will be smeared around the edges. The relation between performance of ASTR systems with respect to these parameters was evaluated and compared to an ASR system.

- How does the uncertainty in angle and magnitude of the ambient flow affect the performance for both ASR and ASTR systems?

The flow parameters of the subsurface may come with high uncertainties. Deviations in the direction and magnitude of the expected and actual flow field may decrease the effectiveness of an ASTR system. ASR systems are not affected by the angle of the ambient flow since it has an injection and extraction at the same point. To reflect on the practical application of ASTR systems, the influence of the angle and groundwater velocity will be evaluated with respect to ASR systems.

2. Theoretical framework

Discharge flow rate

Flow of water in porous media is described by Darcy's law (Neuman, 1977). The discharge can vary in time and space due to changes in ambient flow and pumping activity.:

$$Q_x = -K_x A \frac{dh}{dx} \quad \text{EQ 1}$$

Where Q_x is the discharge in x-direction [L^3/T], Kh is the horizontal hydraulic conductivity [L/T], A is the surface area of the porous medium [L^2], dh/dx is the hydraulic gradient in horizontal direction [L/L].

Theis equation

The hydraulic head changes with time during initiation of pumping and extraction. Theis equation provides an analytical solution to transient modelling of the drawdown (Theis, 1935). This formula describes the drawdown in time and space and was adopted from an analogous solution in heat conduction theory (Wang et al., 2004). The is valid for homogeneous and isotropic aquifers with a fully penetrating well.

$$S = \frac{Q}{4\pi t} W(u) \quad \text{EQ 2}$$

Where S is the drawdown [L], Q is the pumping rate [L^3/T], T is the time transmissivity [L^2/T] and W(u) is an exponential integral.

Flow velocity

The flow velocity of water through a porous medium is characterized by its effective velocity. This is defined as the flux of water through a unit area of pore space:

$$V_x = \frac{K_x}{\Theta} \frac{dh}{dx} \quad \text{EQ 3}$$

Where V is the ambient velocity in x-direction, Θ is the porosity of the porous medium (-).

Advection

Advection describes the lateral transport of dissolved compounds in their host fluid. The advection is described as a mass flux of the dissolved compound and depends on the concentration of the solute and the discharge of the host fluid.

$$F_{i-x} = q_x C \quad \text{EQ 4}$$

Where F_{i-x} is the mass flux of solute I in x-direction [M/T], q_x is the specific discharge [L^3/T] in x-direction and C is the concentration (M/L^3) of the dissolved chloride.

Advection dispersion equation

Mechanical dispersion and molecular diffusion are two processes describing the mixing of ambient and injected water at the interface. Mechanical dispersion is caused by irregularities in the subsurface and is influenced by the magnitude of the advection. The porous subsurface describes paths with different lengths and cross sections. This results in deviations in the flow velocity, inducing mixing and the freshwater interface. Molecular diffusion is caused by Brownian movement of atoms (Weissmann et al., 2002). Its contribution to mixing is generally smaller than that of mechanical dispersion but can in practice not be separated. The combined term is described by the hydrodynamical dispersion. This effect is combined with advection in the advection-dispersion equation (ADE) (Bear, 1972):

$$\frac{\partial C}{\partial t} = -V_x \frac{\partial C}{\partial x} + D_L \frac{\partial^2 C}{\partial x^2} - D_T \frac{\partial^2 C}{\partial y^2} + D_V \frac{\partial^2 C}{\partial z^2} \quad \text{EQ 5}$$

Where t is time (T) and D_L, D_T and D_V are the longitudinal, transverse, and vertical transverse hydrodynamical dispersion (L^2/T) in x,y,z direction respectively.

Hydraulic radius

The injection of freshwater over the whole depth of the aquifer with a fully penetrating well, results in a cylindrical volume. The radius of the injection is an important parameter for the interfacial area between fresh and ambient water. When ignoring influences of hydrodynamic dispersion, the hydraulic radius R_h is approximated by:

$$R_h = \sqrt{\frac{V_{inj}}{\Theta \pi D}} \qquad \text{EQ 6}$$

Where V_{inj} is the injected freshwater volume (L^3) and D is the thickness (L) of the aquifer.

Injection and capture zone

The shape of the injection and extraction volumes, or the capture zone, has been modelled with a mathematical approach by Bear and Jacobs (1965) and Ceric and Haitjema (2005). An important parameter to estimate the shape of the extracted volume is determined by the time-of-travel parameter τ (T) for the capture zone of extraction wells (Ceric & Haitjema, 2005), here we assume that this parameter also determines the shape of the injected volume:

$$\tau = \frac{2\pi Q_0^2 t}{\Theta H Q_x} \qquad \text{EQ 7}$$

Where t is the time of injection or extraction (T), Q_0 is the ambient flow rate (L^2/T) and H is the thickness of the aquifer (L).

When $\tau < 0.1$ the capture zone is approximately circular with the origin at the well. When $0.1 < \tau < 1$ the capture zone is still circular, however its origin shifts downgradient by a factor δ:

$$\delta = 0.00278 + 0.652\tau \qquad \text{EQ 8}$$

For $\tau > 1$, a circular approximation is not reasonable. The injection volume takes an ellipsoidal shape and for infinite injection times form a long plume (Figure 3). In this case the capture zone can be approximated by:

$$X = \frac{Y}{tan\left(\frac{2\pi Q_0}{Q_x} Y\right)} \qquad \text{EQ 9}$$

Where X and Y are the corresponding coordinates in the model.

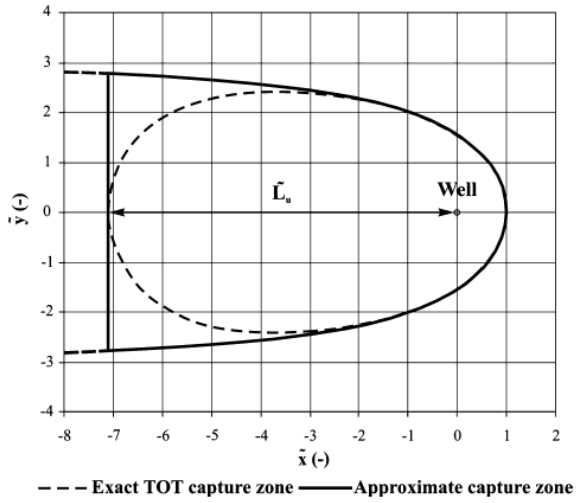

Figure 3. Time of travel capture zone for τ larger than 1. Where L_u is the upstream length from the well to the edge of the injected volume. For infinite extraction times the approximate capture zone is applicable, for shorter extraction times the exact TOT capture zone is more suited from Ceric and Haitjema (2005).

Analytical well positioning

In this study, an estimation of the optimized well position is made. The estimation assumes instantaneous injection of a circular volume around the well at t=0.5*t_{inj} and a circular capture zone due to instantaneous extraction at t=(0.5 t_{inj}+$t_{storage}$+0.5 t_{ext}). The movement of the center of the injection volume is given by:

$$X_{center} = (0.5\, t_{inj} + t_{storage} + 0.5\, t_{ext})\, V_x \qquad \text{EQ 10}$$

Where X_{center} is the x-coordinate (L) of the extraction well, t_{inj} , $t_{storage}$,t t_{ext} are the injection, storage, and extraction times (T) respectively.

Mixing fraction and cutoff

In the subsurface, processes such as dispersion cause the injected freshwater to mix with the ambient groundwater, decreasing the quality and usefulness of the extracted water. Therefore a threshold for 'acceptable' water quality is necessary, which allows discrete classification towards quality of recovered water (Ward et al., 2009). The Mixing Fraction (MF) is a useful parameter that can define the extent of mixing of ambient and injected water that is allowed, without exceeding the cutoff (Ward et al., 2007). The quality of the water is characterized by a relative mixing value of injected and ambient water. This value is defined on an interval between 1 (100% injected water) and 0 (100% ambient water).

$$MF = \frac{C_{amb} - C_{well}}{C_{amb} - C_{inj}} \qquad \text{EQ 11}$$

Where C_{amb} is the ambient concentration (M/L^3), C_{well} is the concentration in the well (M/L^3) at a specific time and C_{inj} is the injection concentration (M/L^3).

Recovery efficiency

The amount of water that can be recovered by an ASR application determines its value for the designed purpose. The Recovery Efficiency, the fraction of water that can be recovered, is the main performance parameter for ASR and ASTR. The extraction in the well is halted when the mixing fraction decreases below a set cutoff. The RE tends to increase when the extraction volume increases, since mixing processes mainly take place at the edges of the injected column and relatively more ambient groundwater will be extracted during the end of the extraction period (van Ginkel et al., 2014; Ward et al., 2007). Low recovery results in a small usable extraction volume, at risk of not satisfying the water demand or not being economically feasible (Zuurbier et al., 2014).

The recovery efficiency can be defined in different ways, here we distinguish between the recovered total volume (RE) and the recovered injected volume (RE_{inj}). The RE represents the volume fraction of acceptable water that is extracted with respect to the injected volume:

$$RE = \frac{V_{ext}}{V_{inj}} \qquad \text{EQ 12}$$

Where V_{ext} is the total extracted volume above the cutoff.

RE_{inj} is the volume of injected water that is recovered through the injection well. This is determined based on MF and extraction rate:

$$RE_{inj} = \frac{t_{ext} Q_{ext} MF}{V_{inj}} \qquad \text{EQ 13}$$

Where t_{ext} is the extraction time (T) and Q_{ext} is the extraction pumping rate (L^3/T).

Ideally, a RE of 1 would be achieved by modelling an AS(T)R system without hydrodynamic and numerical dispersion, when the extraction well is placed at the predicted center of the injection volume. For practical applications, the hydrodynamic dispersion and parameter uncertainties may decrease the RE below 1.

3. Methods and model

3.1 Model

Model settings

As a basis, an existing 3D model by KWR with one well, combined extraction and injection, and ambient flow in MODFLOW 6 (Langevin et al., 2022) is used. The model is operated in FloPy, solving the governing equations of the MODFLOW module in a Python environment (Bakker et al., 2016). MODFLOW 6 contains the groundwater flow and groundwater transport package (Langevin et al., 2022). The advection term is solved using the "TVD" solver. The model is converted to a one-layer 2D top view model, with a separate second well introduced to the system. The function of the priorly combined injection and abstraction well is split, allowing the wells to be separated in space, with the injection well situated at the origin (Figure 4). The wells are fully penetrating over the whole depth of the model. A complete overview of input parameters is given in Table 7.

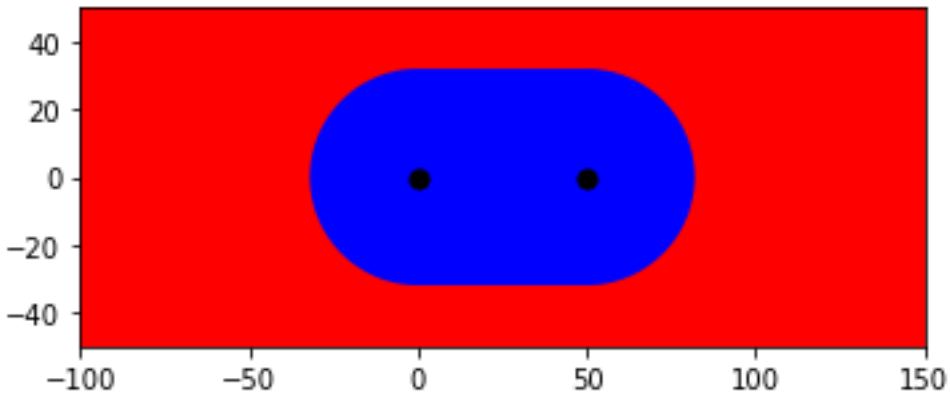

Figure 4. Overview of the refined model area. In blue the highly refined area (0.25 m^2 /cell), in red the slightly refined area (1024 m^2 / cell).Injection well placed on the left, downstream extraction well on the right.

This study is focused on modelling dissolved chloride. This element is a good indicator of the salinity in the water (Boumaiza et al., 2022). WHO and Dutch legislation on drinking water salinity are well substantiated for this element (Rijksoverheid, 2015; WHO, 2003). The WHO norm is less strict than the norm for Dutch drinking water companies. As such, this study aims for the stricter chloride cutoff of 150 mg/L. A concentration of 1000 mg/L and 10 mg/L is assumed for ambient and injected water, respectively. Therefore, the cutoff for acceptable water in terms of MF is 0.86 (EQ 10). By including a small safety factor, the cutoff in the model is set at 0.9, allowing 10% mixing between ambient and injected water. Extraction of water in the model is halted when the MF in the observation well is below this value.

The single-layer model for the study area is homogeneous and isotropic. Constant head boundaries are used for the outer left and right boundaries, such that flow, when present, is from left to right. All spatial units are defined in meters, temporal units are in days. Freshwater is injected in an aquifer during the injection period of 90 days at the start of the simulation. This is followed by a storage period (90 days) in which no pumping takes place. Lastly, an extraction period is modelled, whose length depends on total recovery and spans a maximum of 90 days. The model checks after each extraction day whether the cutoff, indicating the acceptable chloride concentration, is exceeded. If so, extraction is terminated and a rest period is created to complete the 90 days. The full simulation thus spans three quarters of a year, an injection, storage, and extraction/rest period, each lasting 90 days. The time discretization of 1 day per step, does not allow for distinction in changes of RE smaller than 0.011. At this resolution, it is likely to find well positions with similar RE, even though well distances differ. In these cases, to optimize the well position more accurately and increase the refinement of the model, the RE_{inj} rather than RE, is leading in determining the optimized well positioning.

The well distance is defined as the distance between injection and extraction well, for ASR systems this distance is 0 m. For an ASTR setup the optimized well distance is found through iteration steps. The model starts by simulation an ASR setup. Then it takes a guess of the optimized well distance (EQ 10) and takes this value as the starting distance (Figure 5). The stop value prevents the model from running infinitely when parameters are chosen such that the RE is 0 at any given location. Its value is the addition of the start value and three times the first step size. The model runs a simulation with an extraction well at the start value. Then, in the iteration step, the model starts running new simulations with changing well distances at an interval of 8 m until the stop value is reached or until the RE decreases, indicating a temporary optimum in the previous run. When an optimum is found, the interval is halved and runs again over 2 well distances surrounding the optimal well distance (Figure 5). This continues until the interval is equal to the cell size in the refined area, presenting the final optimum well distance.

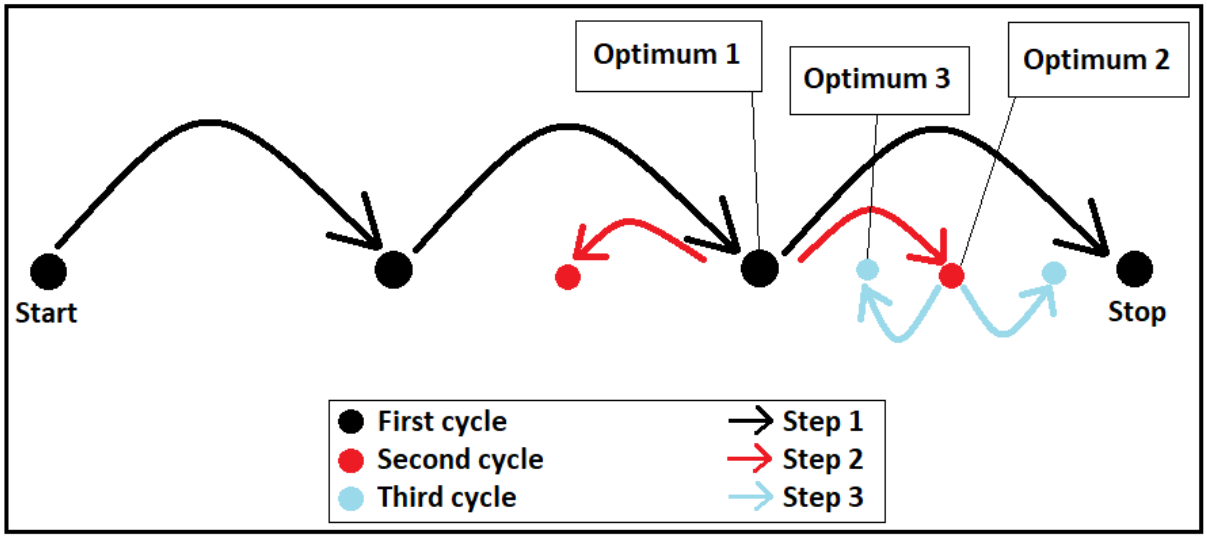

Figure 5. Optimization process for the extraction well distance downstream with respect to the injection well. The model iterates over decreasing step size to find the optimal well positioning.

Nested grid

The base grid consisted of 25 columns and 13 rows of square cells with a length of 128 m. The model dimensions are 3200 m, 1664 m, 20 m in x,y,z-directions, respectively. The model was equipped with a nested grid rather than a structured grid. These grids allow a local refinement of the grid, by overlaying a new grid on cells of choice. This decreases the number of cells in the model non transport zone by eliminating the stretched cells at the middle of the sides of the grid (Figure 6). Any refinement shape can be implemented. Furthermore, the boundaries of the model can be located further from the refined transport domain without demanding larger increases in number of cells to decrease the boundary effects on flow conditions.

Nested grids require specification of refinement polygons. In this study, two refinements were added to the base grid. The first refinement was a square stretching over 512 m in length and 384 m in width, with a cell size of 32 m. The second refinement, the high-resolution zone, had a stadium shaped geometry, dividing the grid in cells of size 0.5 m (Figure 4). The circular edges of the stadium shape resemble the shape of the injection volume. This grid is adjusted depending on the injection volume and shape. This feature eliminates more cells that are not used for transport and decreases the runtime by 10-80% for the different scenarios.

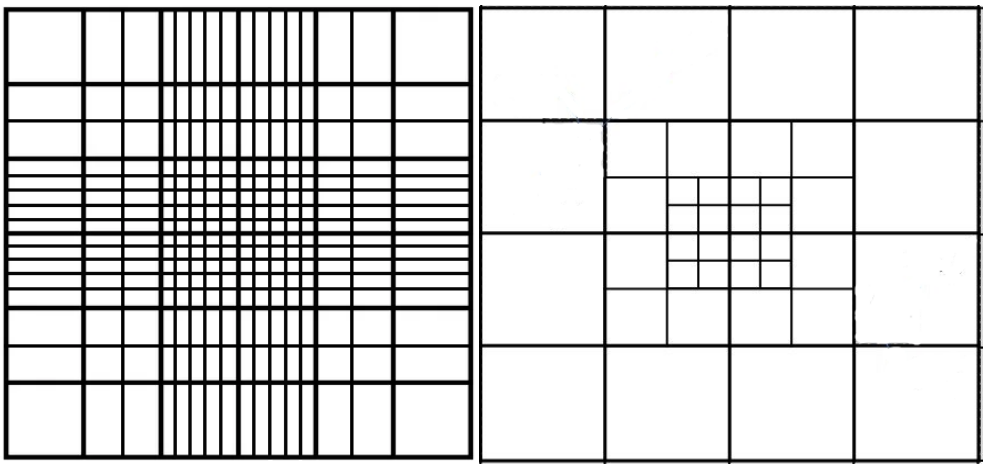

Figure 6. Two types of model grids. On the left is a structured grid with predefined distances between columns and rows. On the right is a nested grid, where specific cells are split into symmetrical sub cells.

3.2 Scenarios

The RE and optimized well positioning of the ASR systems is evaluated based on four parameters, hydrodynamic dispersion, ambient flow, injection volume, the angle between groundwater flow direction and the plane of the wells (Table 1). The ambient flow range of 0-100 m/y at an interval of 20 m/y is used in all scenarios. Different injection volumes are evaluated in each scenario from 10-100 thousand m^3, with pumping rates of 111-1,111 m^3/day. Each simulation runs an additional ASR setup with the extraction well located at the injection well. This results in a base scenario and two extra scenarios, each evaluating one of the remaining parameters: dispersion and angle. A general overview of the simulations in this study is shown in Table 1 and an overview of the range of all input parameters is given in Table 7.

Base scenarios

In the base scenario, the RE and optimized well distance for ASTR systems are evaluated based on the ambient flow range of 0-100 m/y. The injection volumes were 10, 40, 70 and 100 thousand m^3. The longitudinal dispersivity (α_L) was set at 0.5 m and the was no angle between the flow velocity and the plane of the two wells.

Dispersivity scenarios

In this scenario, the longitudinal dispersivity (α_L) is evaluated on an interval from 1e-4 m to 5 m. The corresponding transverse dispersivity (α_T) was defined as:

$$\alpha_T = 0.1 * \alpha_L \qquad \textit{EQ 14}$$

These scenarios were evaluated with two injection volumes: 10 and 100 thousand m^3.

Angular dependency scenarios

This scenario is formed by two sub scenarios, the two scenarios were simulated to determine the influence of an angle between ambient flow and the plane of the two wells on the RE. In the first scenario, a situation is mimicked, where surface well placement is limited in the flow direction (Figure 7, left). The angle (β) was set at 5 and 20 degrees, respectively. The iteration of the well positioning in X-direction is given by a start and stop value like the base scenario and optimized during the run. The Y-coordinate of the extraction well followed by:

$$Y_{well} = X_{well} * tan\,(\beta) \qquad \textit{EQ 15}$$

In the second scenario, the optimized well distance from the base scenario is used. The angle (β) is then set at 20 degrees (Figure 7, right). This imitates a situation at which the expected flow conditions deviate from the actual conditions. This type of deviation is likely to occur in practical applications, for example due to inaccurate measurements of the flow direction. The coordinates of the extraction well in this scenario were determined by:

$$X_{well} = WD_{optimal} * cos\ (\beta) \qquad EQ\ 16$$

$$Y_{well} = WD_{optimal} * sin\ (\beta) \qquad EQ\ 17$$

Where $WD_{optimized}$, is the optimized well distance (m) of a simulation in the base scenario.

Table 1. Scenario overview with their corresponding parameters. Optimization scenarios at an angle without ambient flow are identical to the no flow scenarios without angle.

Dispersion (m)	Volume (10^3 m3)	Ambient flow (m/y)						Angle (degrees)	Angle uncertainty
0.0001	10	0	20	40	60	80	100	0	No
0.001	100	0	20	40	60	80	100		
0.1	10	0	20	40	60	80	100		
	100	0	20	40	60	80	100		
0.5	10	0	20	40	60	80	100		
	40	0	20	40	60	80	100		
	70	0	20	40	60	80	100		
	100	0	20	40	60	80	100		
	10	0	20	40	60	80	100		Yes
	40	0	20	40	60	80	100		
	70	0	20	40	60	80	100		
	100	0	20	40	60	80	100		
	10		20	40	60	80	100	5	No
	40		20	40	60	80	100		
	70		20	40	60	80	100		
	100		20	40	60	80	100		
	40		20	40	60	80	100	20	
	70		20	40	60	80	100		
	100		20	40	60	80	100		
2	10	0	20	40	60	80	100	0	
	100	0	20	40	60	80	100		
5	10	0	20	40	60	80	100		
	100	0	20	40	60	80	100		

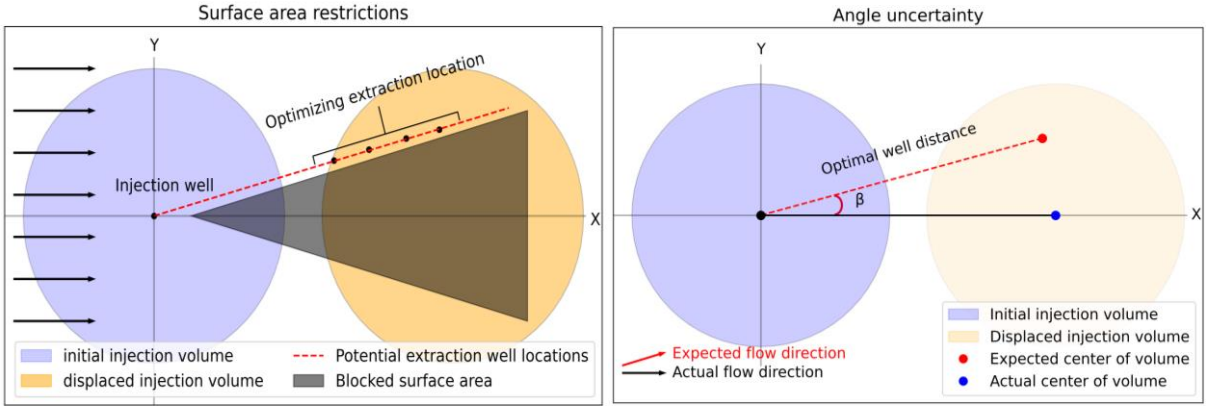

Figure 7. Two scenarios with an angle between the wells and the flow direction, on the left intentional, due to restricted surface area and on the right unintended due to inaccurate measurements of the flow direction.

4. Results

The results of each scenario are described in a separate section. For the dispersivity and angular scenario, the results are compared to findings from the base scenario. The parameters applicable to each specific scenario are highlighted at the beginning of the section Table 2, Table 3 and Table 4.

4.1 Base scenario

Table 2. Parameter overview of the base scenario highlighted in green.

Dispersion (m)	Volume (10^3 m3)	Ambient flow (m/y)						Angle (degrees)	Angle uncertainty
0.0001	10	0	20	40	60	80	100	0	No
0.001	100	0	20	40	60	80	100		
0.1	10	0	20	40	60	80	100		
	100	0	20	40	60	80	100		
0.5	10	0	20	40	60	80	100	0	No
	40	0	20	40	60	80	100		
	70	0	20	40	60	80	100		
	100	0	20	40	60	80	100		
0.5	10	0	20	40	60	80	100	0	Yes
	40	0	20	40	60	80	100		
	70	0	20	40	60	80	100		
	100	0	20	40	60	80	100		
	10		20	40	60	80	100	5	No
	40		20	40	60	80	100		
	70		20	40	60	80	100		
	100		20	40	60	80	100		
	40		20	40	60	80	100	20	
	70		20	40	60	80	100		
	100		20	40	60	80	100		
2	10	0	20	40	60	80	100	0	
	100	0	20	40	60	80	100		
5	10	0	20	40	60	80	100		
	100	0	20	40	60	80	100		

The shape of the injection volumes in the base scenario is dependent on ambient velocity and the ratio of injection rate and depth. Smaller ratios create more oval shapes, whereas the higher ratios result in circular shapes. Without flow the shape of the injected freshwater volumes is circular. High ambient velocities result in less circular volumes with the center more laterally displaced from the well. Figure 8 shows a cycle of the ASTR system with the smallest and largest volume, 10 and 100 thousand m^3, respectively and an ambient velocity of 100 m/y. The injected volumes were not completely recovered, due to mixing and the use of the sharp cutoff of 110 mg/L (Figure 8C).

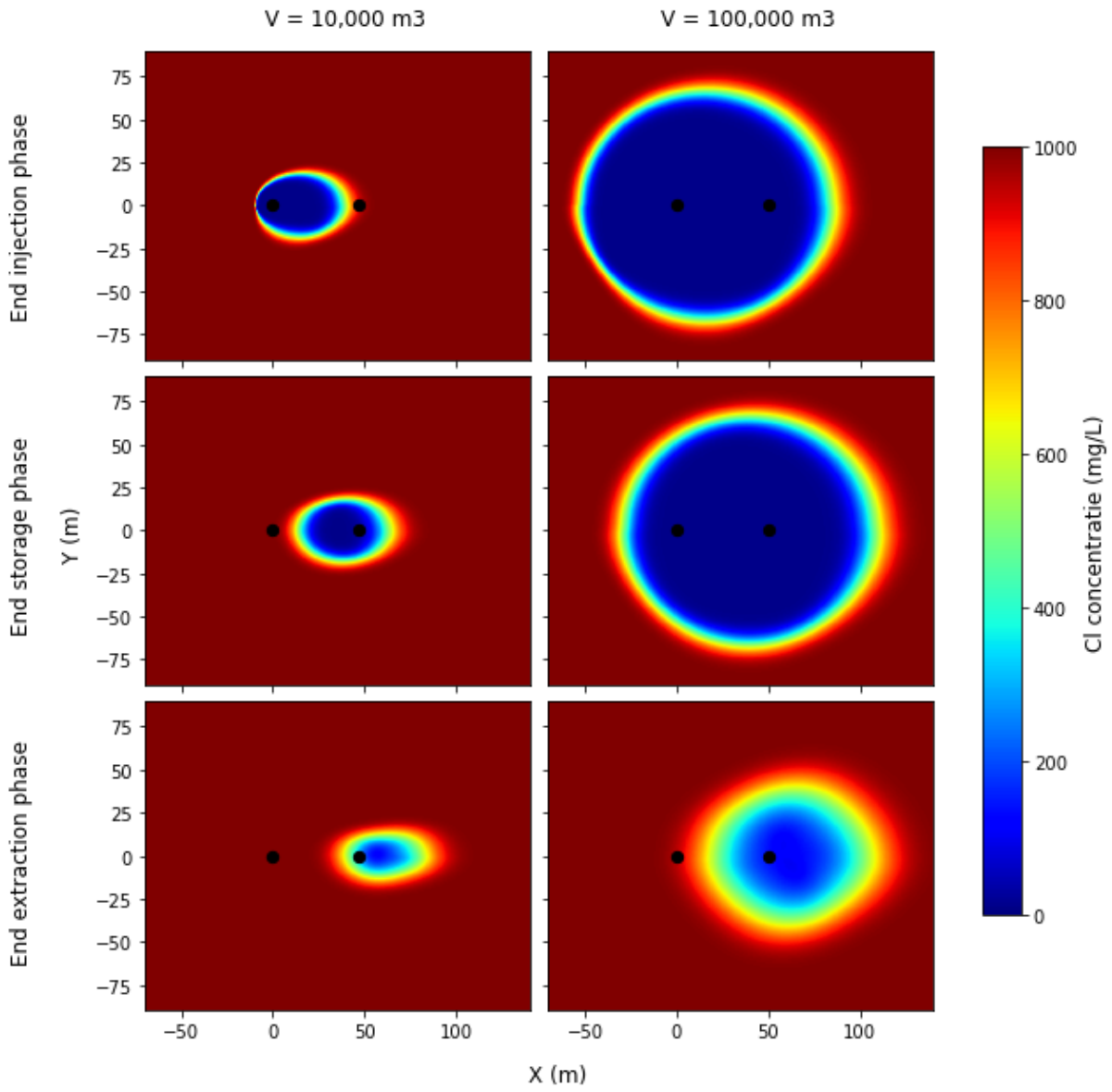

Figure 8. Concentration profiles for optimized well distances where V_{amb}=100 m/y and α_L=0.5 m.

During the injection period, the well induces a change in the flow field around the well (Figure 9A). In concentration terms, the front of the plume stretches in ambient flow direction. When injection is terminated, the local flow field vanishes and becomes uniform, equal to the start of the model (Figure 9B). The dispersion now becomes more apparent on the upstream side of the injection volume (Figure 8B). Throughout the extraction period an inverted change of the flow field is present at the location of the extraction well compared to the injection period (Figure 9C). During the extraction phase, the injected volume remaining in the subsurface shrinks. At the end of the extraction phase for an optimized well distance, a smeared injected freshwater volume remains in the aquifer, where the MF at the center is lower than the cutoff allows for optimized well distances (Figure 8C). Non-optimized distances are characterized by a deep blue low concentration volume remaining in the aquifer (Figure 10). When the chosen well distance is larger than the optimized well distance, this can also be determined from the observation of the MF in the extraction well (Figure 11). After the stop of the extraction at t=220 days, the MF increases again above the cutoff, indicating the passage of a low concentration front over the extraction well.

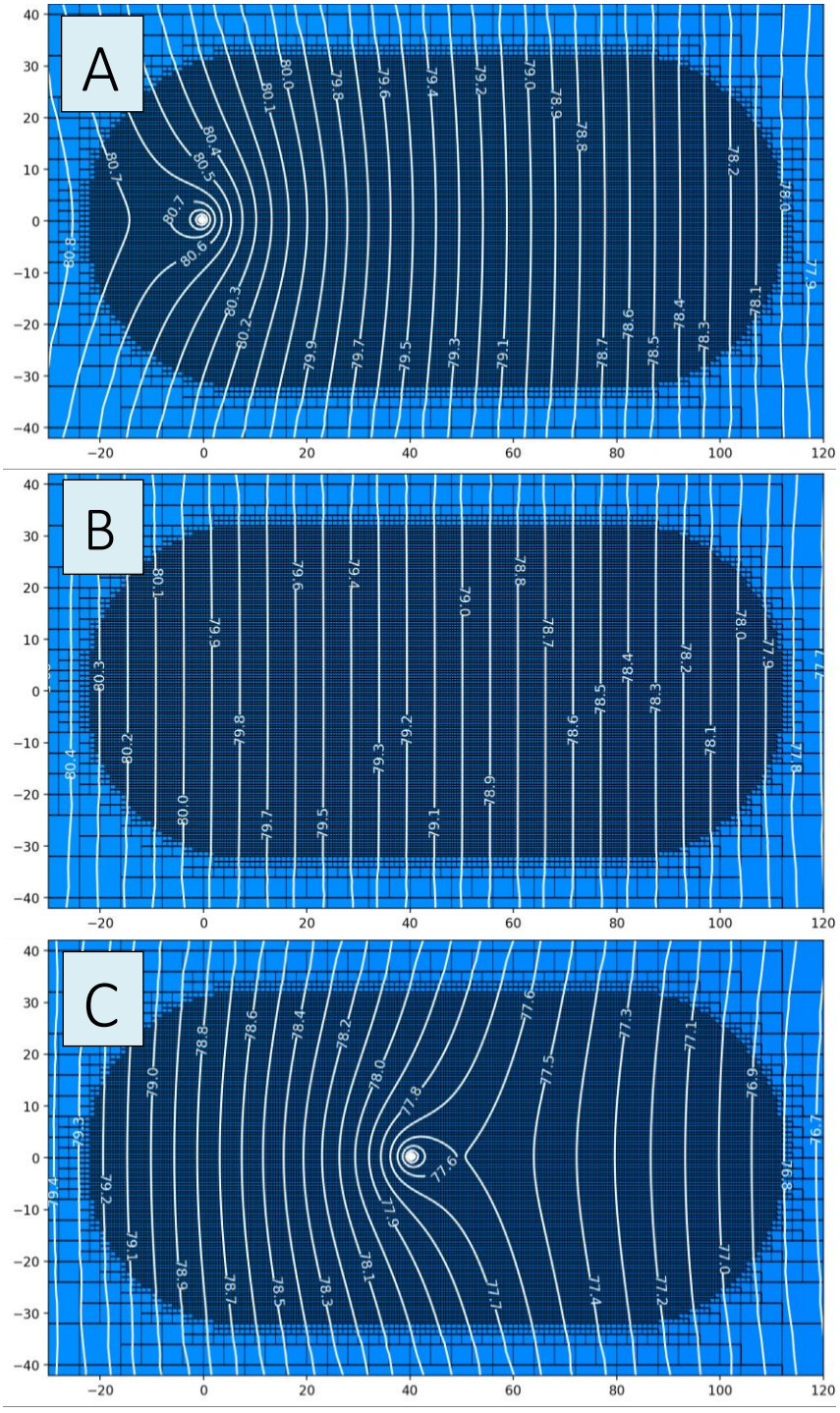

Figure 9. Hydraulic head isolines where V_{amb}=100 m/y, α_L=0.5 m and V_{inj}=10 thousand m^3 during injection (A), storage (B) and extraction (C).

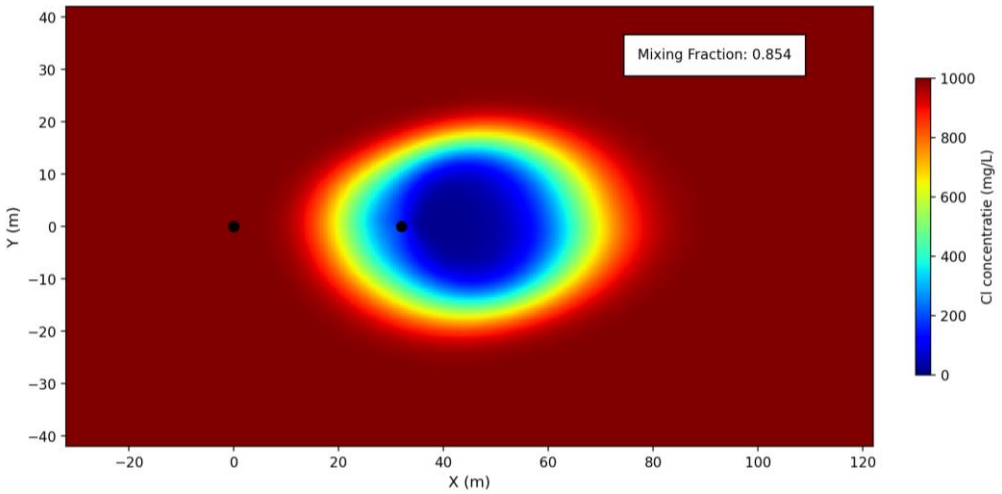

Figure 10. Concentration map of a non-optimized well position (32 m) at the end of the extraction phase for V_{inj}=10 thousand m^3 at V_{amb}=100 m/y. The dark blue spot describes freshwater with chloride concentrations below the cutoff.

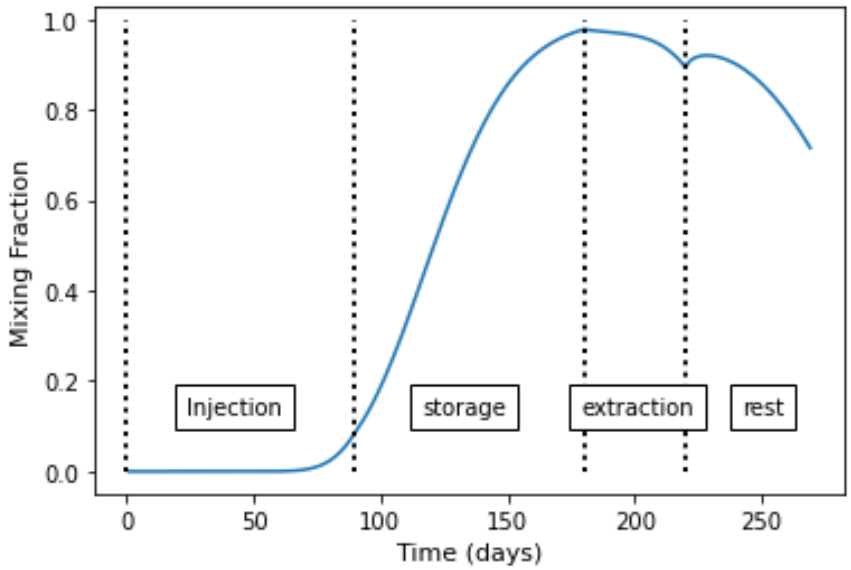

Figure 11. Observed MF in the extraction well at 51.5 m where V_{amb}=100 m/y, α_L=0.5 m and V_{inj}=10 thousand m^3 . Extraction begins at t=180 and stops at t=220.

The optimization process depicted in Figure 12 shows that the optimized well distance increases with ambient velocity. Furthermore, the RE of the no flow simulation is symmetrical around the optimized well distance: 0 m. For simulations with ambient flow the RE is not symmetrical around the optimized distance. Due to the ambient flow, the capture zone will deviate from a circular shape with the well at its center. The downstream deviation from the optimum decreases the RE more than upstream displacement. Combined with the cutoff, which cannot be exceeded, this results in a slightly skewed optimization curve. For volumes of 100 thousand m^3, the decrease in RE due to deviations from the numerically optimized well distance is smaller than for a volume of 10 thousand m^3 (Figure 12). In the large volume simulations, the RE is constant over 2-4 meters, whereas for the smaller volumes this is only 1-2.5 m. The optimum of RE_{inj} is mostly at the smallest well distance of equal RE locations. The optimized well distance is chosen such that quality of the recovered water is the highest among locations with equal total extraction volumes.

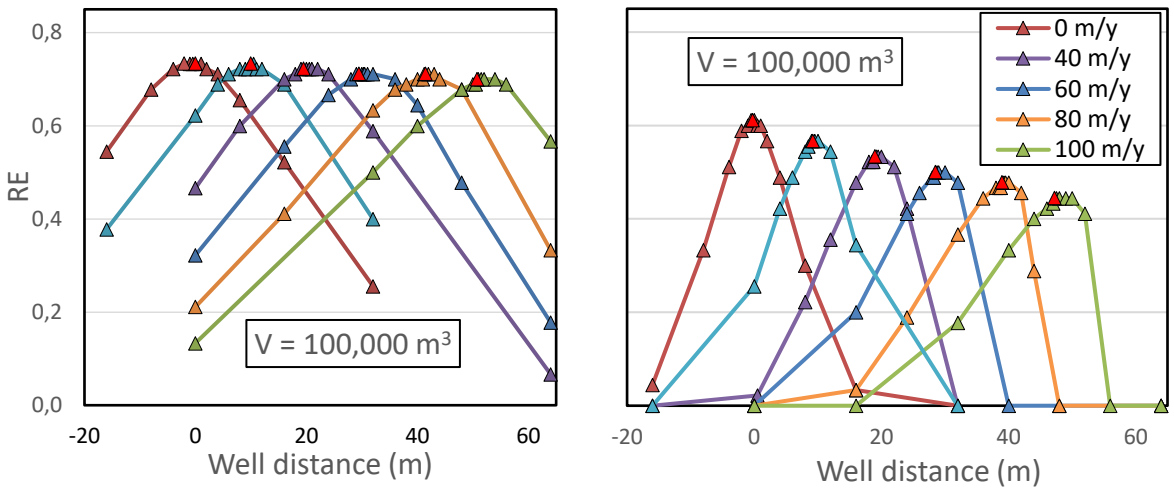

Figure 12. Well distance optimization for ASTR systems where α_L=0.5 m. The red triangle indicates the optimized well distance for each simulation.

Figure 12 describes the relation between the optimized well distance and RE for 10, 40, 70 and 100 thousand m^3 and the analytical estimation of the optimized well distance. The numerically optimized location of the downstream extraction correlates very well with the analytical estimation (EQ 10). At higher ambient flows, deviations of the analytical approach increase, up to 2.1 m for the smallest injection volume (Figure 13). For larger volumes, the optimized well distance at higher ambient velocities is slightly larger than via the analytical approach, 1.2 m, 2.8 m and 1.4 m for volumes of 40, 70 and 100 thousand m^3 respectively. As these deviations are relatively small and both increased and decreased optimized well distance are found, the deviations may be associated with numerical errors.

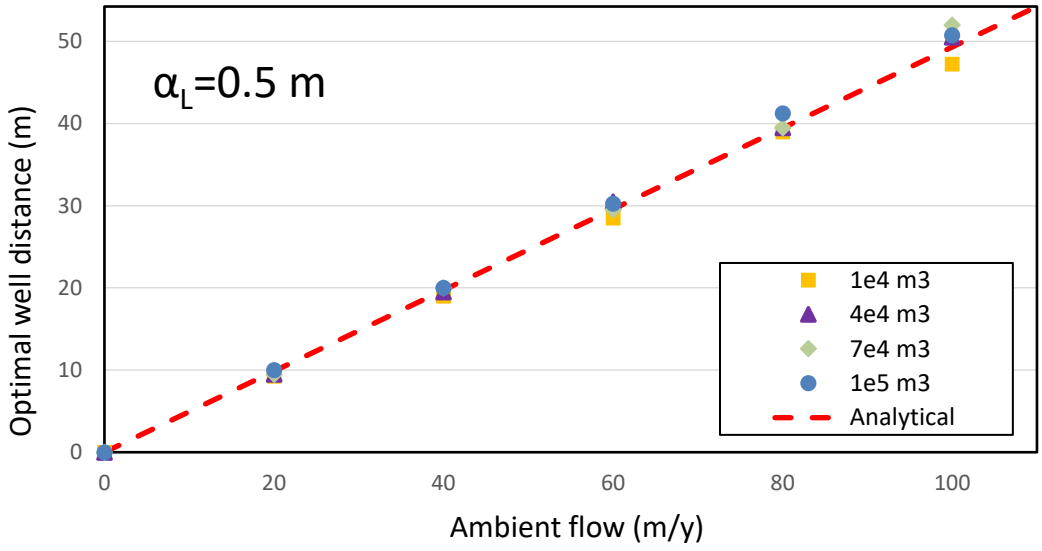

Figure 13. Optimized well distance for base scenarios against ambient velocity. Analytical well distance is constructed by $(0.5*t_{inj}+t_{storage}+0.5*t_{ext})*V_{amb}$, corresponding to a line through the origin with slope 0.4932.

Figure 13 describes the RE of ASR and optimized ASTR systems over an ambient flow of 0-100m/y. Without flow, the optimized well distance was at the origin, thus an ASR system is the most efficient. In all other simulations of the base scenario, where ambient flow >0 m/y, the ASTR system generates numerically higher RE than ASR systems. In simulations with volumes ≤40 thousand m^3 injection volume, the RE of the ASR system at the highest ambient velocity drops to 0, whereas the ASTR system with optimized well distance maintains a RE between 0.44 and 0.62. At an ambient flow of 20 m/y the ASR systems with an injection volume ≥40 thousand m^3 show a RE between 0.49 and 0.61, against 0.68 to

0.73 for ASTR systems. Indicating that, numerically, the larger ASR systems may still be feasible at lower ambient flows.

Increasing ambient flow results in lower RE's for both ASR and ASTR systems (Figure 14). ASR systems, where ambient flow up to 100 m/y and the injection volume ≥40 thousand m^3, show a drop of 0.20 to 0.11 in RE per increase in ambient flow of 20 m/y. In comparison for the optimized ASTR systems under the same conditions, the decrease in RE is 0.01 per decrease in ambient flow of 20 m/y. Showing that under optimized conditions numerical loss in RE can be decreased in the model. In the base scenario, the decrease in RE of optimized ambient flow simulations is stronger for the smallest volume than the largest volume, a decrease of 0.167 and 0.033 for injection volumes of 10 and 100 thousand m^3, respectively. For the smallest volume, the decrease in RE from no flow to 100 m/y of 0.17 is a 27% drop of the total RE compared to the ASR system without ambient flow. For the volumes 40-100 thousand m^3, this decrease in RE is 0.07-0.03 a relative 10-5% of the RE in the no flow scenario. These differences likely originate from the larger R_h for larger volumes.

Figure 15 describes the RE of ASR and ASTR systems under different ambient flow conditions, normalized to the R_h of the injection volumes. When considering the relative volume over ambient velocity, the decrease of the RE in the ASR system shows a trend among all base scenario simulations (Figure 15). Without flow, V_{amb}/R_h is 0, and RE's are not equal among the different volume simulations. When V_{amb}/R_h is higher than 2, all ASR scenarios tends to a RE of 0 (Figure 15). At this ratio, the lateral movement of the injected volume is equal to the radius of the injection volume. The extraction well will immediately extract ambient water at the start of the period, instantly stopping extraction. For the volume of 40 thousand m^3 the RE drops to 0 at a V_{amb}/R_h ratio of approximately 2.5 (Figure 15). This increased ratio may arise from a combination of factors. Firstly, the number of datapoints in this region is limited, potentially overestimating the R_h ratio at which the first reaches a RE of 0. Secondly, the injection is not instantaneous, therefore the volume is deformed into a more ellipsoidal shape due to ambient flow. As such, the hydraulic radius may not be a good approximation to determine the horizontal length of the injection volume.

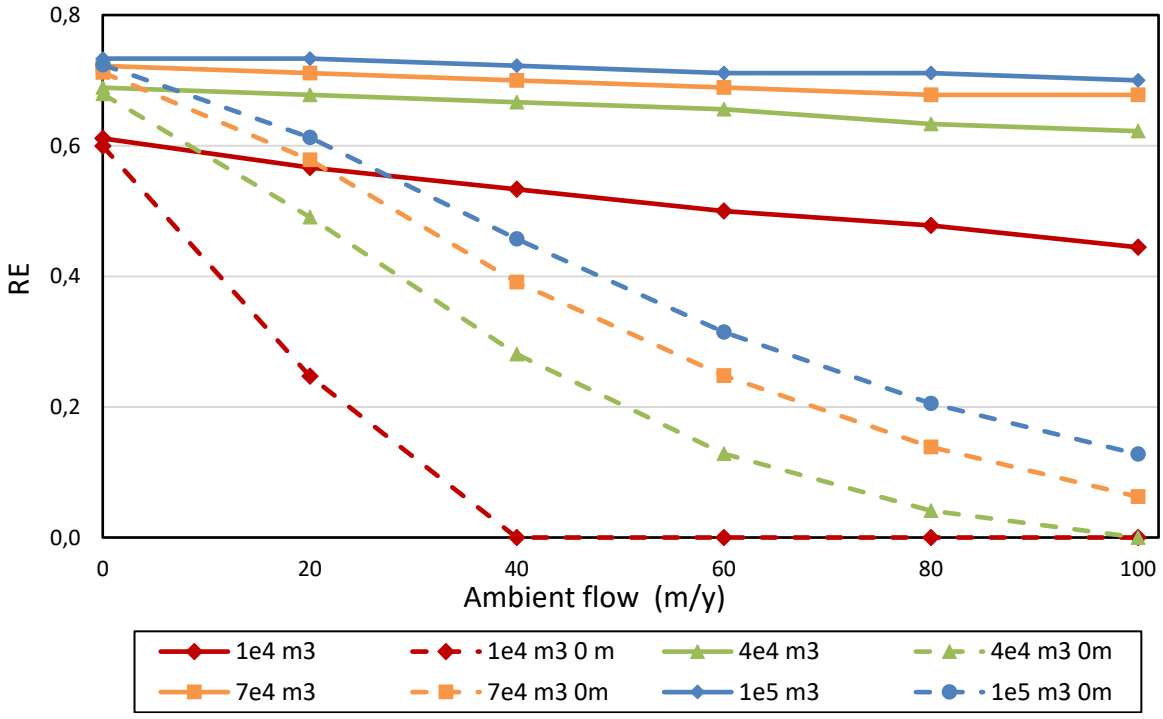

Figure 14. Ambient velocity against RE for 4 different injection volumes. Each solid line represents an optimized ASTR system, each dotted line corresponds to an ASR system.

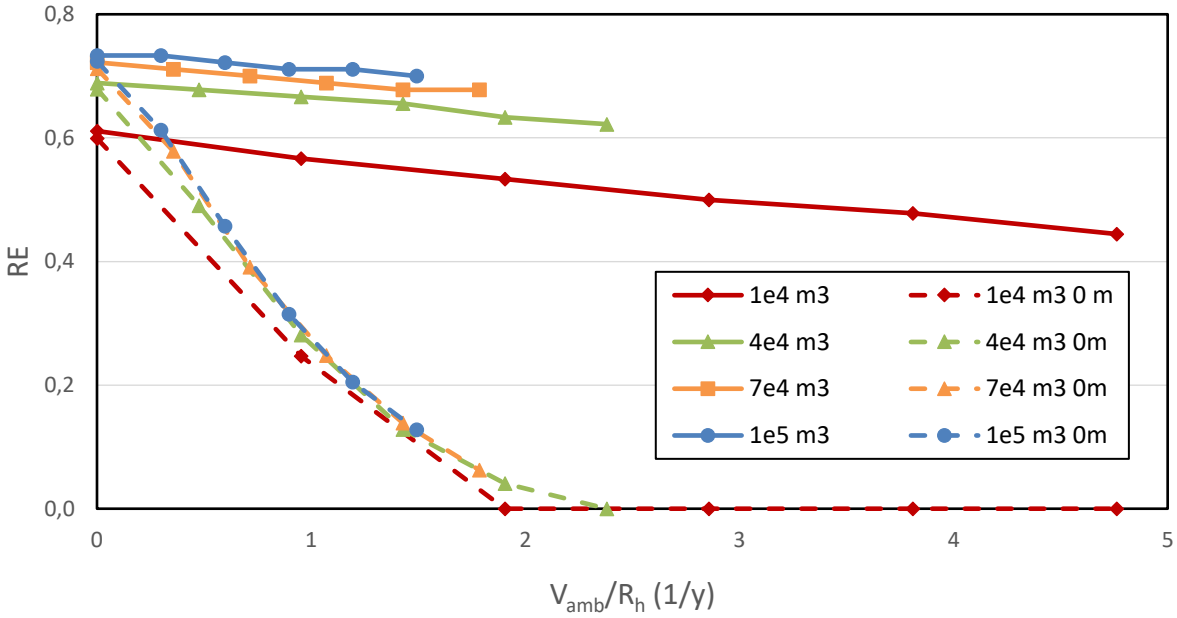

Figure 15. RE vs ratio of ambient velocity over hydraulic radius (R_h). Solid lines represent optimized ASTR systems, dotted lines represent ASR systems.

Figure 16 shows the added value of the ASTR setup by the absolute difference in RE between an ASR and ASTR system. Without ambient flow the optimized well distance is 0 m and thus equal to an ASR system. Increasing ambient flow positively correlates with the absolute gain in RE for an optimized ASTR system over an ASR system. The ASTR system with a volume of 40 thousand m^3 at an ambient flow of 100 m/y has the highest gain in RE (0.6) and thus benefits most from the optimization. Theoretically, the smallest systems are expected to have more benefit from optimizing the well distance, since their V_{amb}/R_h ratio quickly approaches 2. However, the net gain in RE tops for the smallest volume at an ambient flow of 40 m/y. At this point, the relative gain in RE from Figure 17 becomes more important. This figure indicates the performance of the ASR system against the ASTR system under similar conditions. The RE of the ASR system with the smallest volume decreases quickly to 0, whereas the optimized ASTR system still recovers up to 52% of the injected freshwater volume. When ambient flow further increases, the total RE of the ASTR system decreases as described before based on Figure 14 and Figure 15, thereby explaining the decreasing trend of the smallest volume in Figure 16. In the base scenario, decrease in RE between volumes is generally larger than the decrease due to ambient flow. For volumes ≥40 thousand m^3, the inevitable loss in RE of ASTR systems due to ambient flow is approximately a factor 10 smaller than the difference between ASR and ASTR systems (Figure 14 and Figure 17).

For simulations with parameter sets within in the base scenario, numerically optimizing the well distance for ASTR systems is effective in maintaining high RE and if ambient flow is present ASTR systems are preferred over an ASR system when only taking into account the RE. Especially ASR systems with an injection volumes of 10 thousand m^3 show to be vulnerable to ambient flow, whereas larger injection volumes with larger R_h show a more stable RE in the base scenario.

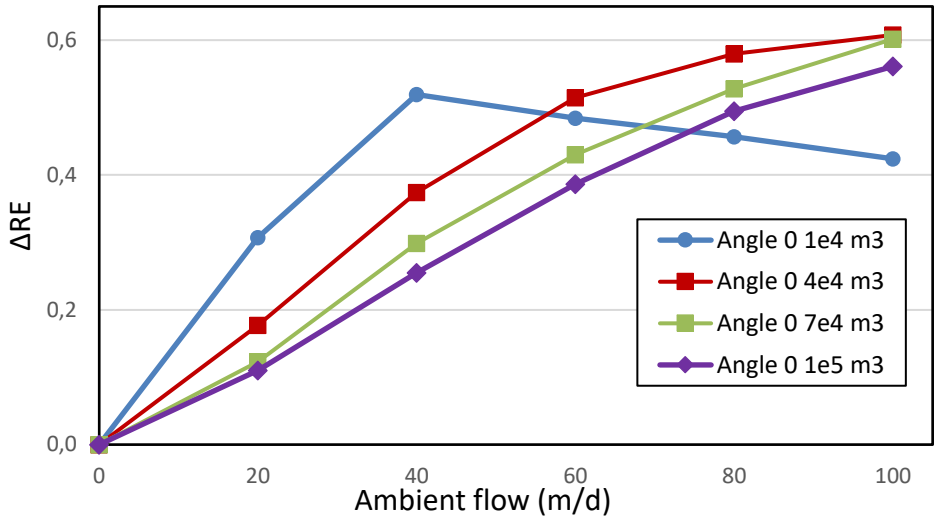

Figure 16. Net gain in RE for an optimized ASTR system with respect to an ASR system where α_L=0.5 m.

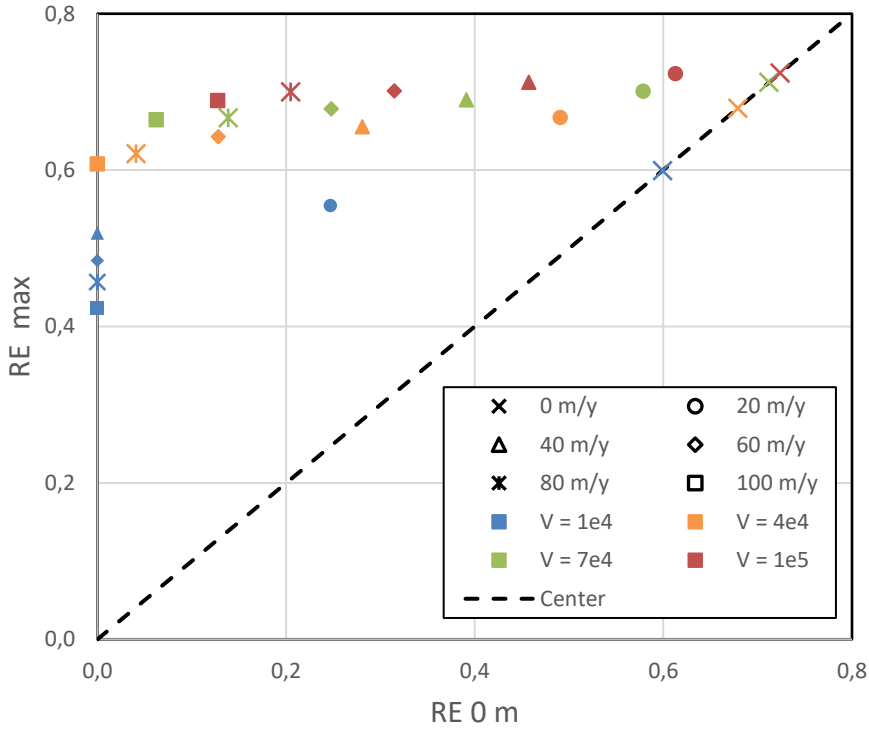

Figure 17. Relative performance of an optimized ASTR system vs and ASR system where α_L=0.5 m. Datapoints are grouped by volume and ambient flow.

4.2 Dispersivity scenario

Table 3. Parameter overview of the dispersion scenario.

Dispersion (m)	Volume (10^3 m3)	Ambient flow (m/y)						Angle (degrees)	Angle uncertainty
0.0001	10	0	20	40	60	80	100	0	No
0.001	100	0	20	40	60	80	100		
0.1	10	0	20	40	60	80	100		
	100	0	20	40	60	80	100		
	10	0	20	40	60	80	100		
	40	0	20	40	60	80	100		No
	70	0	20	40	60	80	100		
	100	0	20	40	60	80	100		
0.5	10	0	20	40	60	80	100	0	Yes
	40	0	20	40	60	80	100		
	70	0	20	40	60	80	100		
	100	0	20	40	60	80	100		
	10		20	40	60	80	100	5	No
	40		20	40	60	80	100		
	70		20	40	60	80	100		
	100		20	40	60	80	100		
	40		20	40	60	80	100	20	
	70		20	40	60	80	100		
	100		20	40	60	80	100		
2	10	0	20	40	60	80	100	0	No
	100	0	20	40	60	80	100		
5	10	0	20	40	60	80	100		
	100	0	20	40	60	80	100		

This scenario evaluates the effect of dispersion for a volume of 10 and 100 thousand m^3 on RE, optimal well positioning and the difference in RE between ASR and ASTR systems. A range of $0.0001 \leq \alpha \leq 5$ m was evaluated.

The optimization curves in Figure 18 are similar to the curves Figure 12 in the base scenario. The trends in Figure 12 and Figure 18 are similar, with the steeper decreases for small volumes compared to the large volumes. The non-symmetrically decreasing RE's left and right of the optimized well positioning, were found in all optimization curves except for α=0.1 m and a volume of 100 thousand m^3. This exception is mainly due to the lack of datapoints, arising from a more efficient numerical optimization method (5.1 Decrease optimization time).

As ambient flow increases, the traveled distance of the injection volume increases. This increases the differences in path length, expanding the area of the injected volume, but simultaneously decreasing the MF in a larger area at the edges of the freshwater volume. Figure 18 also describes the importance of the optimization. The RE remains constant in most situations for 1-2 meters, for small volumes. However, outside this range the RE of non-optimized ASTR systems drops quickly to 0.

When comparing the RE for α = 0.1 and α = 2 m an absolute decrease under similar conditions (Figure 18). Increasing dispersion thus negatively affects the RE of the ASR and optimized ASTR system. With

smaller dispersion, less mixing occurs at the edge of the volume during the injection phase and the storage phase, creating a steeper gradient at the edges of the injection volumes (Figure 19). Larger dispersion causes ambient groundwater to reach the well faster than without dispersion, decreasing the time to reach the cutoff concentration (Figure 19). Because the system becomes more sensitive to mixing with ambient water, the optimization of the location of the extraction well becomes more important in regions with higher dispersion.

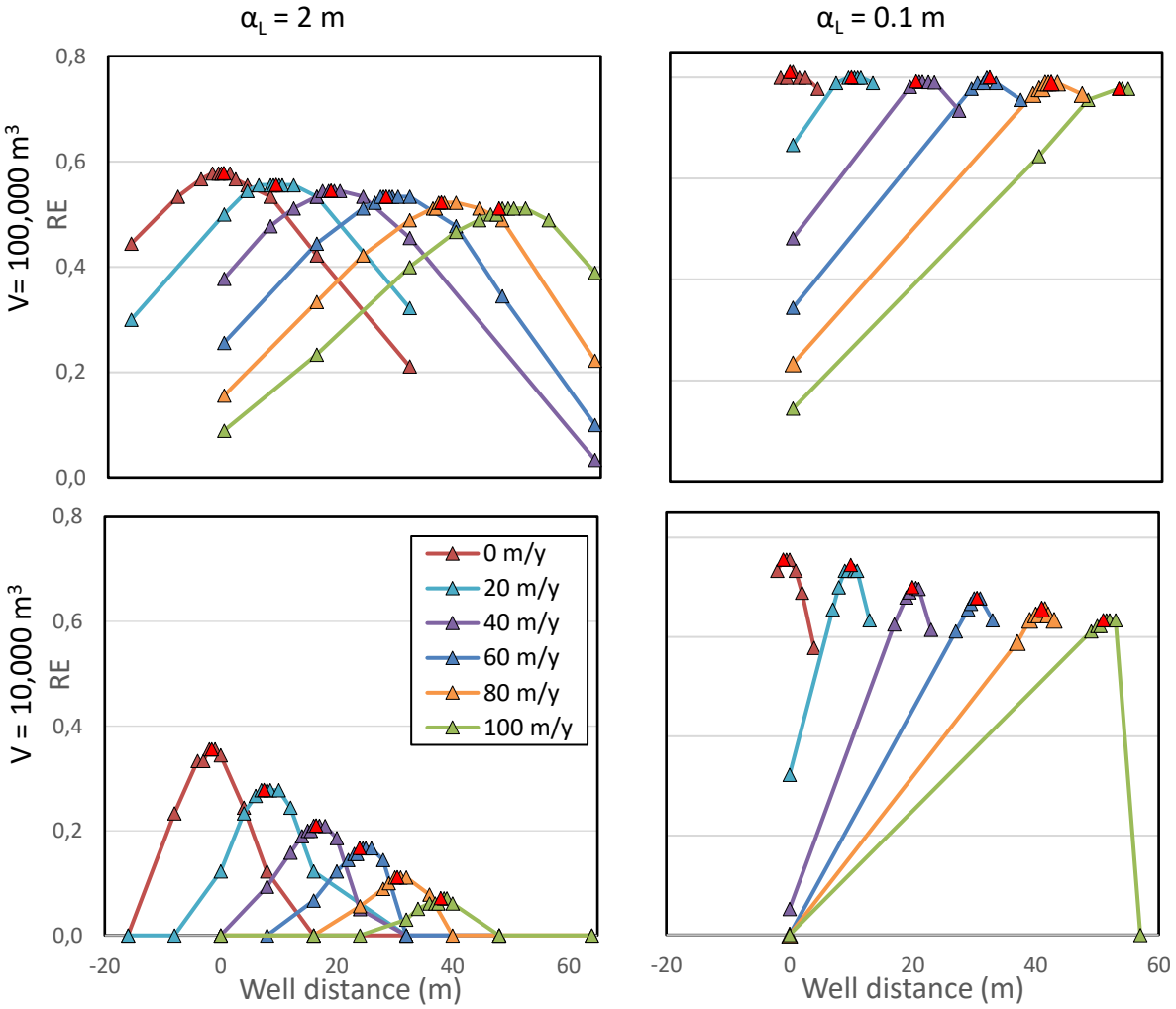

Figure 18. Optimization curve where V_{amb}=100 m/y, α_L=2 m and V_{inj}=100 thousand m^3 (A) and V_{inj}=10 thousand m^3 (B), the red triangle indicates the optimized well distance of a scenario

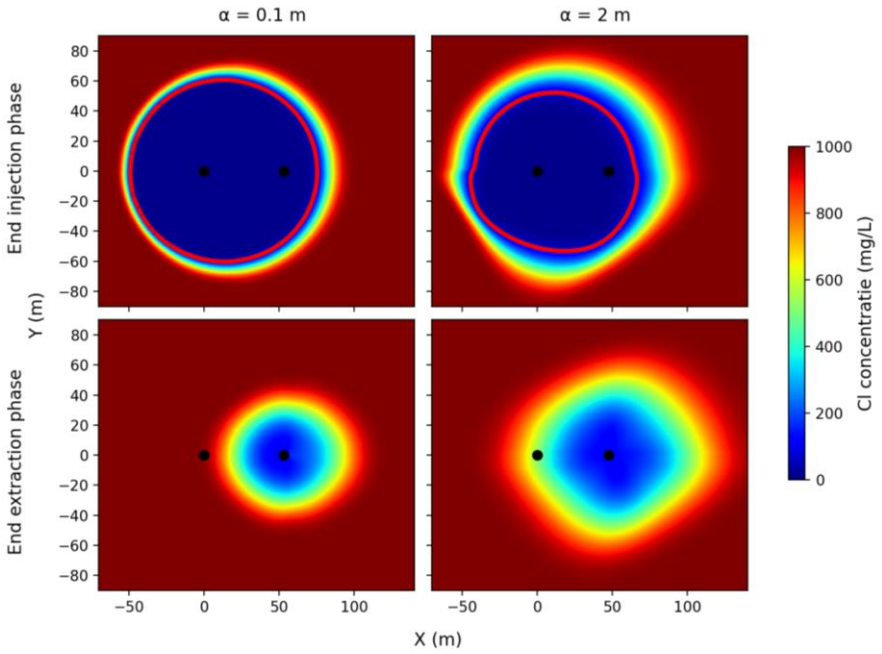

Figure 19. Concentration maps m for an optimized ASTR system at the end of injection and extraction phase, where V_{amb}=100. The red line indicates the injected volume within the cutoff concentration.

The analytical distance becomes less accurate for α deviating from 0.5 m (Figure 20). For α > 0.5 m, the analytical estimation overestimates the numerically optimized well distance, but for α < 0.5 m the optimized well distances are underestimated. The deviations between the optimized ASTR system and the analytical approach are depicted in Figure 21. For ambient flow > 0 m/y, and injection volume of 100 thousand m^3 and α > 0.5 m, the optimized well distance becomes smaller, between 0.8 m and 4.3 m depending on ambient flow. For a volume of 10 thousand m^3 and α = 2 m, the optimal well distances are 1.9 and 11.3 m shorter than the analytical approach, for ambient flow of 20 and 100 m/y, respectively (Figure 21). For α = 5 m with a volume of 10 thousand m^3, no injected water could be recovered above the cutoff for either ASR or the optimized ASTR, indicated by the markers on the x-axis of Figure 20. For α < 0.5 m and an injection volume of 10 thousand m^3, the optimized ASTR well distance is between 0.14 and 1.7 m longer than the analytical estimate. For α < 0.5 m and an injection volume of 100 thousand m^3, this deviation is between 0.14 and 3.7 m.

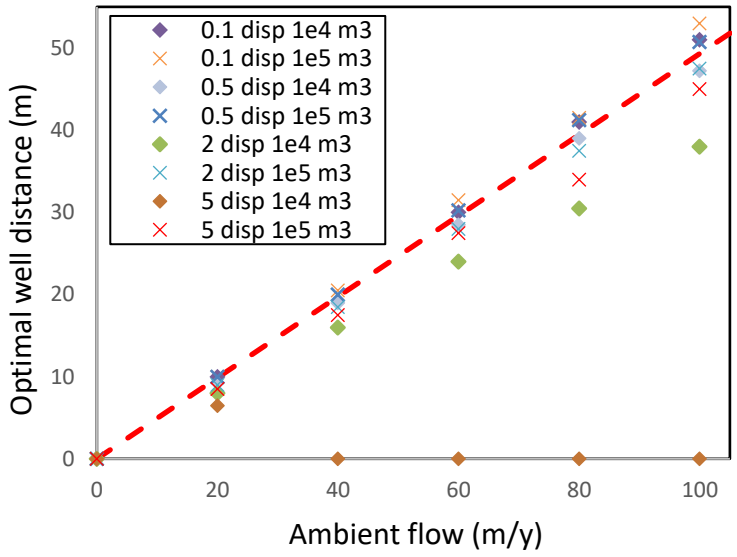

Figure 20. Optimized well distances for different dispersion simulation with respect to the analytical approach.

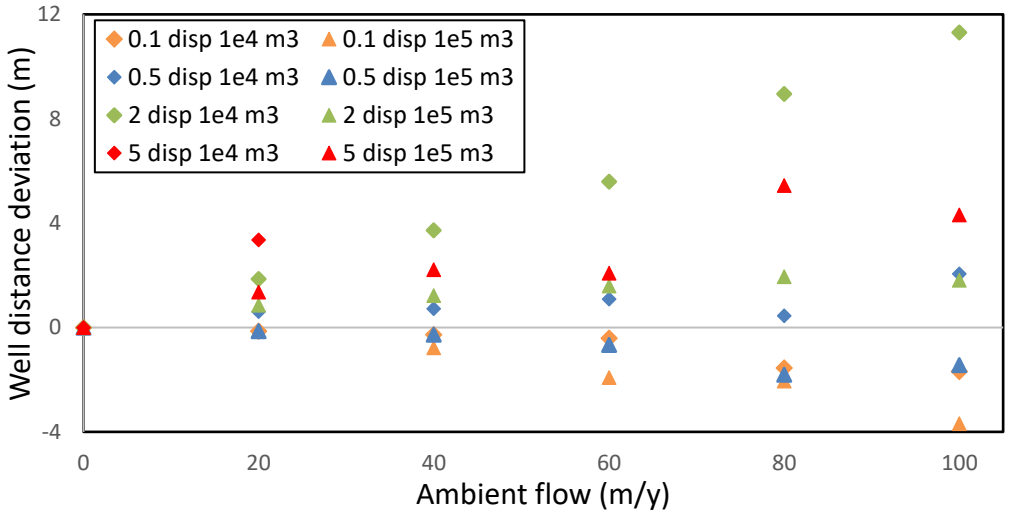

Figure 21. Deviation of the optimized ASTR system with respect to the analytically estimated optimal well distance, for 0.1 ≤ α ≤ 5 m and 0 ≤ V_{amb} ≤ 100 m/y. Positive numbers indicate an overestimation of the optimized well distance by the analytical well distance.

The negative effect of dispersion on the RE is the most impactful when the ambient flow in the subsurface is high (Figure 22). Furthermore, with decreasing volume, the mixing effects due to the dispersion increase. When α is normalized with respect to the R_h, the simulations with ambient flow <40 m/y show minimal deviations in RE, up to 0.06 (Figure 22, right). This indicates that at least for lower ambient flows, the dispersion effects scale with R_h. Figure 23 displays the RE of the optimized and non-optimized dispersion scenarios for volumes of 10 and 100 thousand m^3. For the smaller volume with a dispersion of 5 m and an V_{amb} >40 m/y the RE is 0 even after optimization (Figure 23B). This is a net drop of 0.60-0.78 in RE, depending on ambient flow, compared to the scenario with low dispersion. For larger systems, the RE decrease due to higher dispersion is 0.40-0.46 and almost constant over changing ambient flow velocities (Figure 23A).

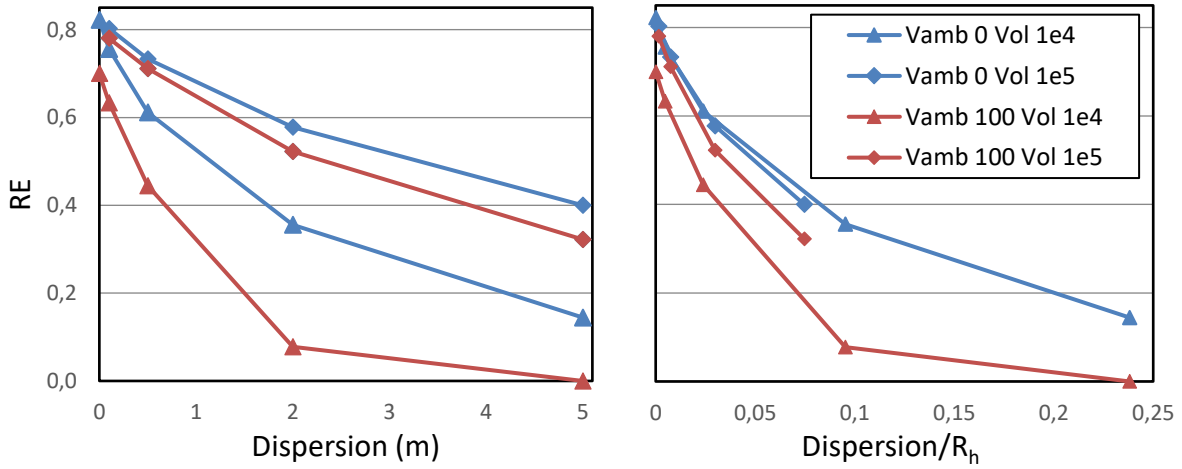

Figure 22. RE of optimized ASTR systems against dispersion (left) and against dispersion normalized to hydraulic radius (right).

Figure 23 describes the evolution of the RE of ASR and optimized ASTR systems for 0.0001 m ≤ α ≤ 5 m. For an injection volume of 10 thousand m^3 the RE of the ASR system decreases to 0 at a ratio for R_h/V_{amb} between 2 and 3. For an injection volume of 100 thousand m^3 the RE of the ASR systems does not reach 0 within the chosen parameter set. The trend is, however, similar to the ASR systems of the larger smaller volume. In the optimized simulations the RE remains relatively stable over the range of R_h/V_{amb} ratios with constant dispersion. For example, the decrease in RE for an injection volume of 10 thousand m^3 and α = 0.0001 m is 0.12. However, when increasing dispersivity the RE decreases steeply. Without

ambient flow, this drop is 80% and 50% of the total RE for the small and large volume respectively in the optimized scenarios when dispersion increases from 0.1 to 5 m.

The change in RE can also be evaluated from the perspective of ambient flow within the dispersion scenario (Figure 23). For an injection volume of 100 thousand m^3, the decrease in RE over the range of ambient flow values is increasing with dispersion, from 0.03 with a dispersion of 0.1 m to 0.09 in the scenario with a dispersion of 5 m. For the small injection volume, the same trend of increasing loss in RE is shown up to a dispersion of 2 m, where the decrease in RE varies from 0.12 to 0.28. The exception in this trend is at α = 5 m. This can be explained by the low RE at V_{amb} = 0 m/y (0.136), defining the maximum drop over the range of ambient flows.

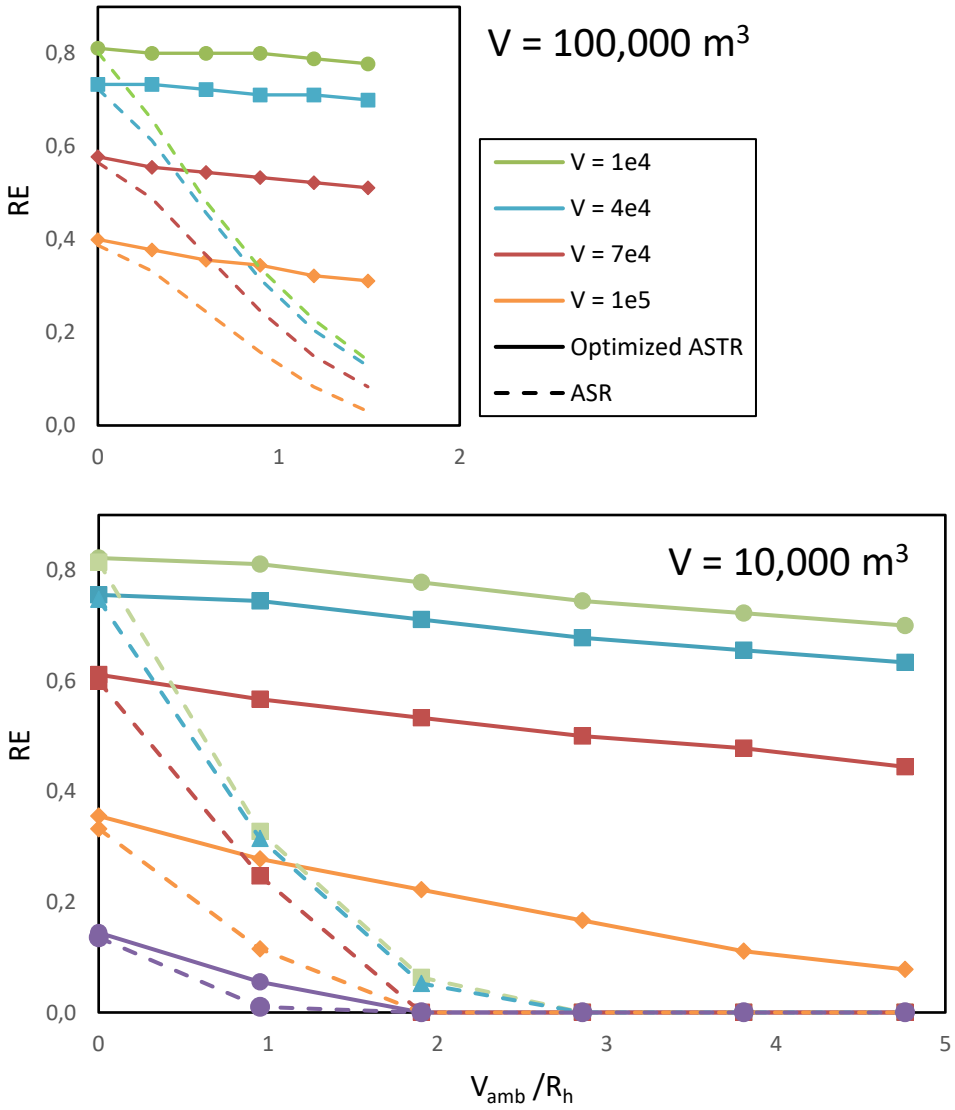

Figure 23. Ambient flow/hydraulic radius against RE for multiple dispersivity values and V_{inj}= A: 100 thousand m^3, B: 10 thousand m^3.

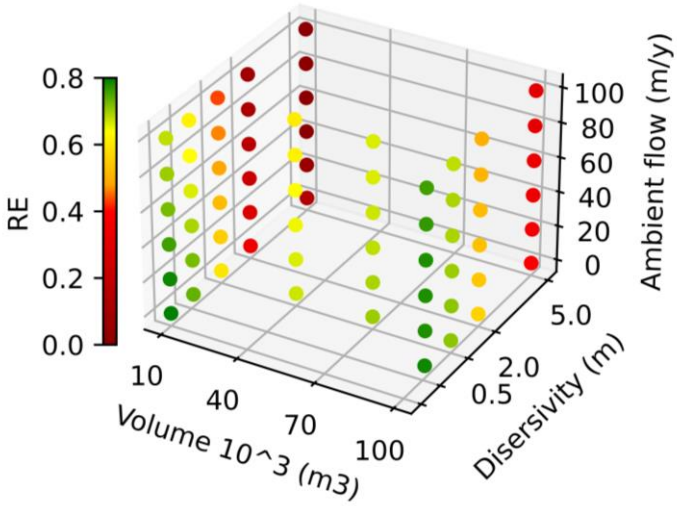

Figure 24. RE of the optimized ASTR system sorted on volume, dispersion (0.0001, 0.1, 0.5, 2 and 5 m) and ambient flow.

So far in this scenario, injection volume, ambient flow and dispersion have been shown to influence the RE of AS(T)R systems. Figure 24 summarizes these parameters with respect to RE of the optimized well. The RE shows a negative correlation with dispersion and ambient flow and a positive correlation with the injection volume. Figure 25 summarizes the relative and net gain in RE due to the optimization of the ASTR system, similar to Figure 17 in the Base scenario. With increasing ambient flow, optimization becomes more important. For smaller volumes the RE quickly decreases to 0 for the non-optimized scenario, whereas for the optimized scenario the RE can still be up to 0.73 (V = 10 thousand m^3, V_{amb} = 40 m/y and α = 0.0001). The decrease in RE over higher dispersion is expressed clearly, a drop in RE of on average 0.66 and 0.44 between 0.1 and 5 m dispersion for an injection volume of 10 and 100 thousand m3 respectively.

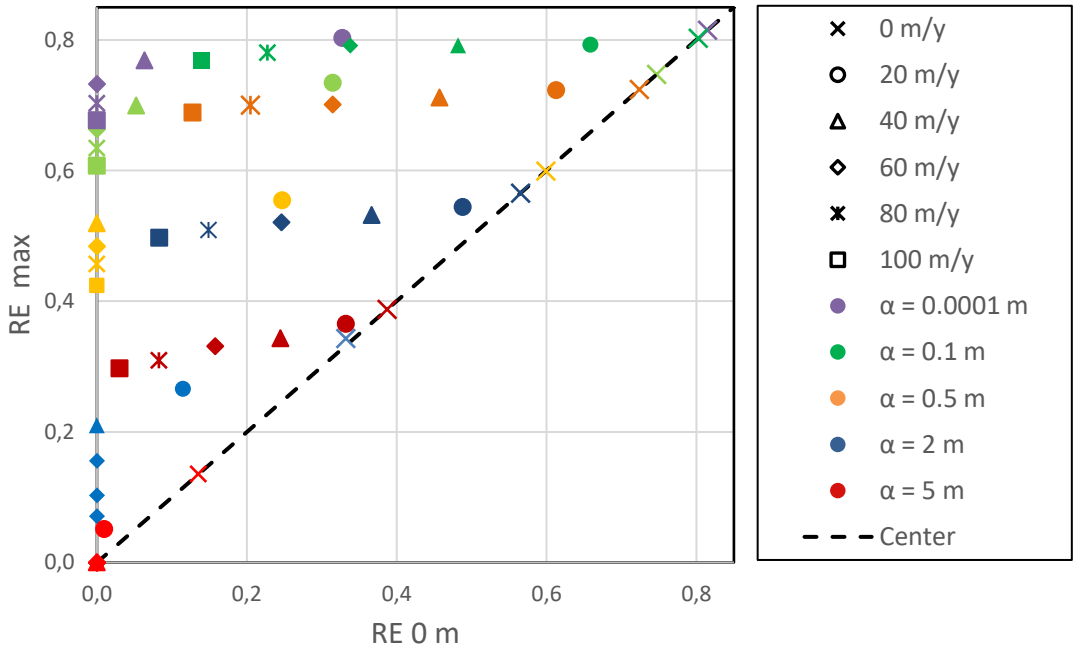

Figure 25. Relative change in RE of the optimized well distance with respect to the ASR system grouped by dispersivity values. Dark shades of α are volumes of 100 thousand m^3 and light shades correspond to volumes of 10 thousand m^3.

4.3 Angular effect

Optimization scenario

Table 4. Parameter overview of the angular optimization scenario.

Dispersion (m)	Volume (10^3 m3)	Ambient flow (m/y)						Angle (degrees)	Angle uncertainty
0.0001	10	0	20	40	60	80	100	0	No
0.001	100	0	20	40	60	80	100		
0.1	10	0	20	40	60	80	100		
	100	0	20	40	60	80	100		
0.5	10	0	20	40	60	80	100		
	40	0	20	40	60	80	100		
	70	0	20	40	60	80	100		
	100	0	20	40	60	80	100		
	10	0	20	40	60	80	100		Yes
	40	0	20	40	60	80	100		
	70	0	20	40	60	80	100		
	100	0	20	40	60	80	100		
	10		20	40	60	80	100	5	No
	40		20	40	60	80	100		
	70		20	40	60	80	100		
	100		20	40	60	80	100		
	40		20	40	60	80	100	20	
	70		20	40	60	80	100		
	100		20	40	60	80	100		
2	10	0	20	40	60	80	100	0	
	100	0	20	40	60	80	100		
5	10	0	20	40	60	80	100		
	100	0	20	40	60	80	100		

This scenario describes the intentional introduction of an angle between the flow field and plane of the wells (Figure 7 Left). The y-coordinate of the extraction well follows from EQ 15. The angle between the flow field and the plane of the injection and extraction well moves the extraction well away from the center of the injection volume (Figure 7, left). All simulations without ambient flow result in no deviations from the base scenario, due to their symmetry. Therefore, this section does not contain a reflection on simulations without ambient flow.

Figure 26 shows the concentration maps of a volume of 10 and 100 thousand m^3 at an angle of 20 degrees. Numerical modelling showed that a large part of the injected volume, especially below the x-axis is not recovered, due to ambient water approaching the well. The least favorable scenario is for highest angle, the smallest volume (10 thousand m^3) and highest ambient flow (100 m/y) and is depicted in Figure 26. In this simulation, the vertical deviation from the extraction well location to the center of the injection volume is maximal relative to the R_h. When ambient flow is smaller, the distance between the center of the injection volume and the injection well at $t=t_{ext}$ decreases. As a result, the deviation from the x-axis decreases, bringing the extraction well closer to the center of the injection volume. This decreases the loss in RE due to the introduction of an angle.

The optimization curves in Figure 27 indicate that the smaller volume becomes more vulnerable to deviations in the well distance compared to the simulations without angle in the base scenario. Overall, the decrease in RE with ambient flow for the scenarios with an angle (0.12-0.58) is larger than for the base scenario (0.03-0.17).

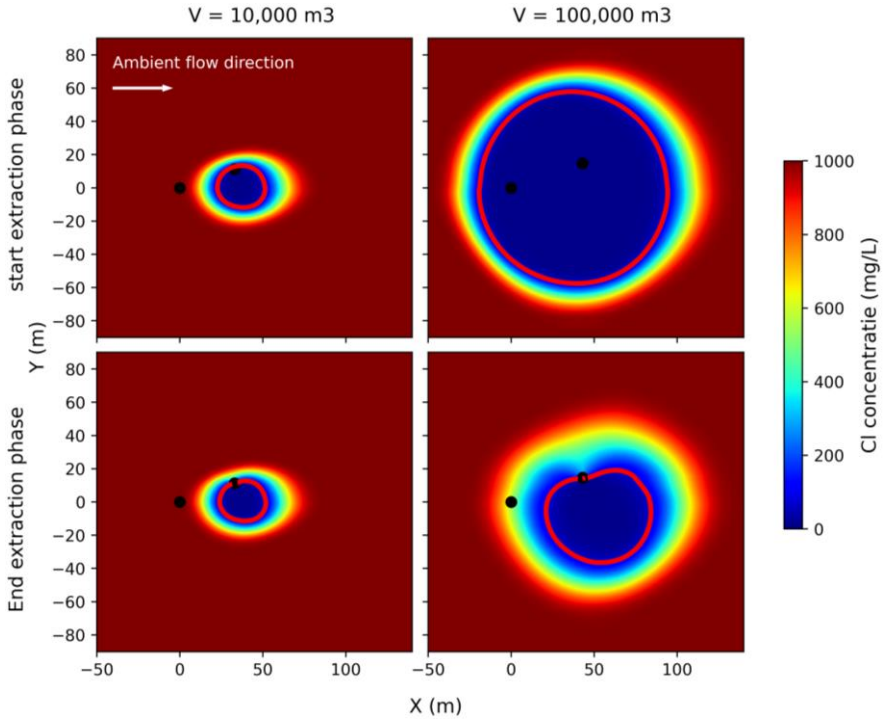

Figure 26. concentration maps of optimized ASTR systems at an angle of 20 degrees, V_{amb}=100 m/y and α_L=0.5 m at the start and end of extraction. The red line indicates the injected volume within the cutoff concentration.

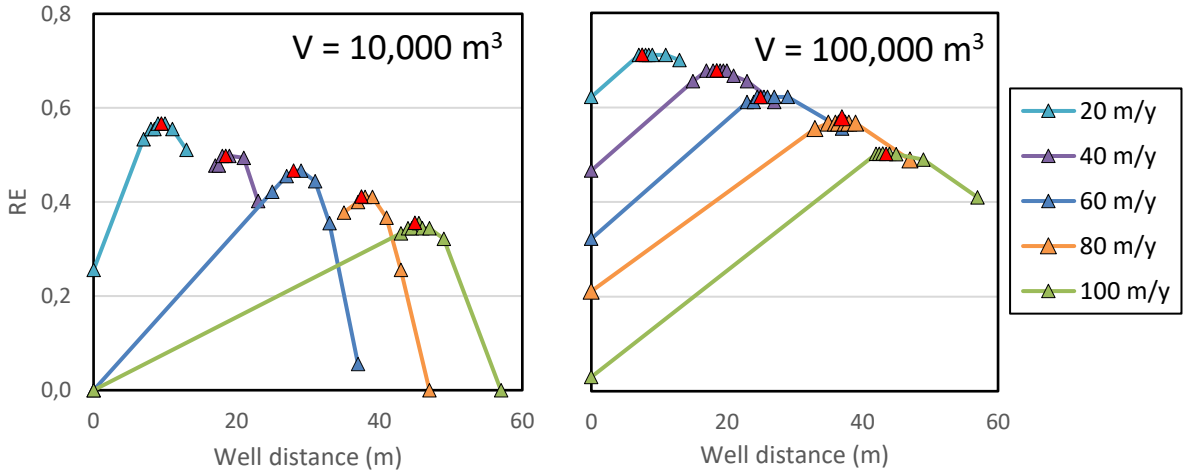

Figure 27. Well distance optimization for ASTR systems where α_L=0.5 m and an angle of 20 degrees. The red triangle indicates the optimized well distance for each simulation.

Figure 28 summarizes the total distance between the wells of the optimized ASTR systems for four volumes and angles of 5 and 20 degrees. For small angles the analytical well distance generally underestimates the optimum well distance. This is because the x-coordinate of the optimized ASTR system for 0 and 5 degrees are comparable (0.5-1.5 m difference). With the small angle, this results in a longer distance between injection and extraction well. As the angle increases the optimum well distance becomes smaller, especially for smaller volumes. This is explained by movement of the freshwater volume: without angle, the extraction well is placed such that the center of the injection volume moves directly towards the injection well and the extraction well can be placed slightly

downstream. When a large angle is introduced, the center of the well does not pass over the extraction well. Reducing the time before ambient water infiltrates becomes more important than capturing the capturing the first front of freshwater. Therefore, at higher angles it is preferred for the extraction well to have an x-coordinate smaller than that of the center of the injection volume (Figure 7, left). For an injection volume of 10 thousand m^3 this results in a 16 m shorter optimized distance than the analytical estimation.

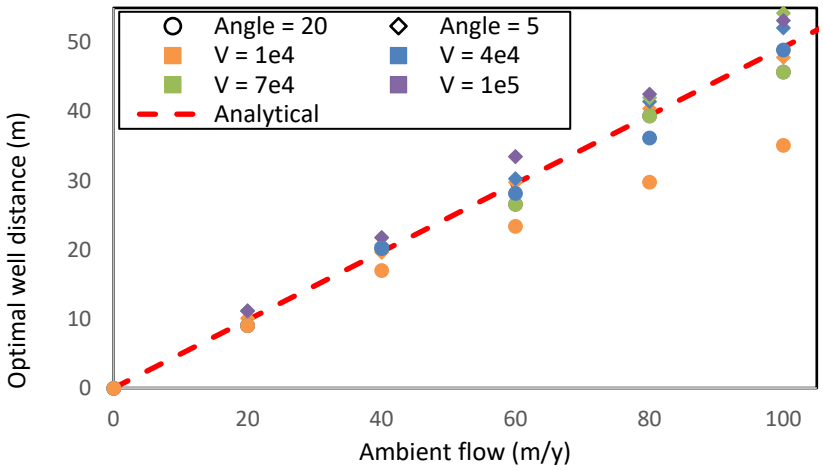

Figure 28. Optimal well distance between injection and extraction well of ASTR systems with an angle of 5 and 20 degrees.

For ASTR with ambient flow, the RE is increasingly reduced when introducing larger angles. Figure 29 describes this decrease. The ambient flow serves as a magnifier of the angular effect, the higher ambient flow the larger the loss in RE. For the most sensitive case, an injection volume of 10 thousand m^3 with an angle of 20 degrees and high ambient flow, there is an RE drop of 0.4 (Figure 29). When looking in an absolute perspective only 3% of the injected volume is recovered (Figure 30). For larger volumes the change in RE for an angle of 20 degrees at 100 m/y is only 0.19. At ambient velocities of 20 m/y the RE loss by introducing an angle is 0.05 and 0.02 for small and large volumes respectively.

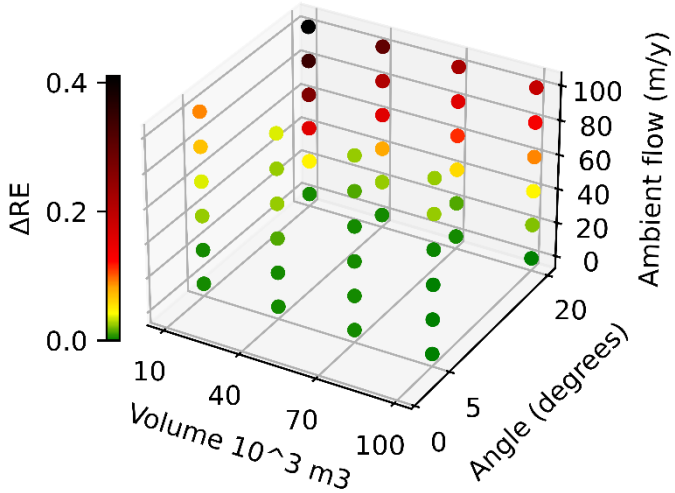

Figure 29. Deviation in RE with respect to the no angle scenario for different injection volumes and ambient flows

The RE of the well is highly dependent on the R_h of the injection volume, when introducing an angle to the model. Large volumes under conditions in this scenario result in the largest R_h. This trend is confirmed in Figure 30, where increasing volumes have increased RE. The smallest volumes decrease to

RE's below 0.38 when ambient flow is increased to 40 m/y. The larger volumes in similar flow conditions present RE's below 0.51 and 0.68 for volumes of 40-100 thousand m^3.

The RE's of an injection volume of 40 thousand m^3 at ambient flows > 60 m/y are 0.02-0.2 smaller than for a small volume (10 thousand m^3) at an ambient flow of 20 m/y (Figure 30). This originates from a both increased injection volume and ambient flow. Higher volumes generally result in larger hydraulic radii, but with increasing ambient flow, the τ value increases (EQ 7). The injection volume becomes more stadium shaped, which decreases the cross-sectional length despite the larger injection volume.

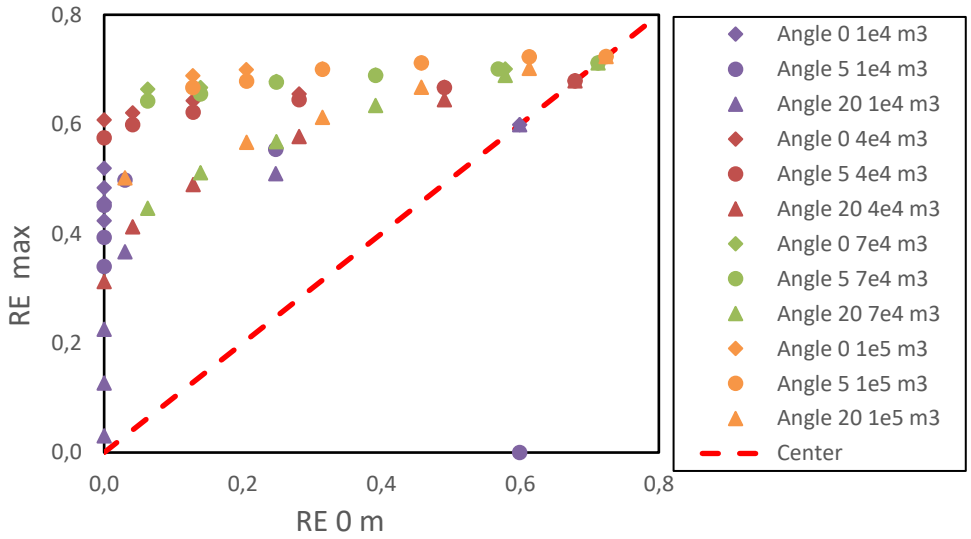

Figure 30. Relative RE of optimized ASTR systems with respect to ASR systems, Where V_{amb}= 0-100 m/y and β=0-20.

Well placement in practice

Table 5. Parameter overview of the scenario with uncertainty in the angle of the groundwater flow direction.

Dispersion (m)	Volume (10^3 m3)	Ambient flow (m/y)						Angle (degrees)	Angle uncertainty
0.0001	10	0	20	40	60	80	100	0	No
0.001	100	0	20	40	60	80	100		
0.1	10	0	20	40	60	80	100		
	100	0	20	40	60	80	100		
	10	0	20	40	60	80	100		
	40	0	20	40	60	80	100		
	70	0	20	40	60	80	100		
	100	0	20	40	60	80	100		
0.5	10	0	20	40	60	80	100		Yes
	40	0	20	40	60	80	100		
	70	0	20	40	60	80	100		
	100	0	20	40	60	80	100		
	10		20	40	60	80	100	5	No
	40		20	40	60	80	100		
	70		20	40	60	80	100		
	100		20	40	60	80	100		
	40		20	40	60	80	100	20	
	70		20	40	60	80	100		
	100		20	40	60	80	100		
2	10	0	20	40	60	80	100	0	
	100	0	20	40	60	80	100		
5	10	0	20	40	60	80	100		
	100	0	20	40	60	80	100		

As described in the Optimization scenario above, the introduction of an angle decreases the performance of the ASTR system inevitably. In this paragraph, the accidental introduction of an angle for the base scenarios is presented and no optimization of the ASTR system is performed. The optimized well distances from the base scenarios are taken and reflect the distance between injection and extraction well. The angle with the flow direction is 20 degrees and the coordinates of the well position are determined EQ 16 and EQ 17.

As the accidental angle is introduced into the system, the horizontal well distance decreases, and increasing the vertical distance from the center of the injected volume. Figure 31 shows difference in optimized well distance between simulations optimized at an angle of 20 degrees and the ones where an accidental angle is introduced, due to uncertainties in the flow conditions. This gives an insight on the loss due to limited knowledge of the subsurface. For ambient flows <60 m/y, the difference is up to 2 m, if we relate this to Figure 27, the losses in RE are between 0.01 and 0.08, for volumes of 10 and 100 thousand m^3, respectively.

The horizontal deviation of the well distance at 20 degrees with respect to the optimized well distance at 0 degrees is 0.52 m per ambient flow step of 20 m/y. Figure 31 shows that for smaller volumes the

introduction of an accidental angle increases the deviation in optimized well distance steadily over higher ambient flows. As a result, the RE will be low (Figure 30).

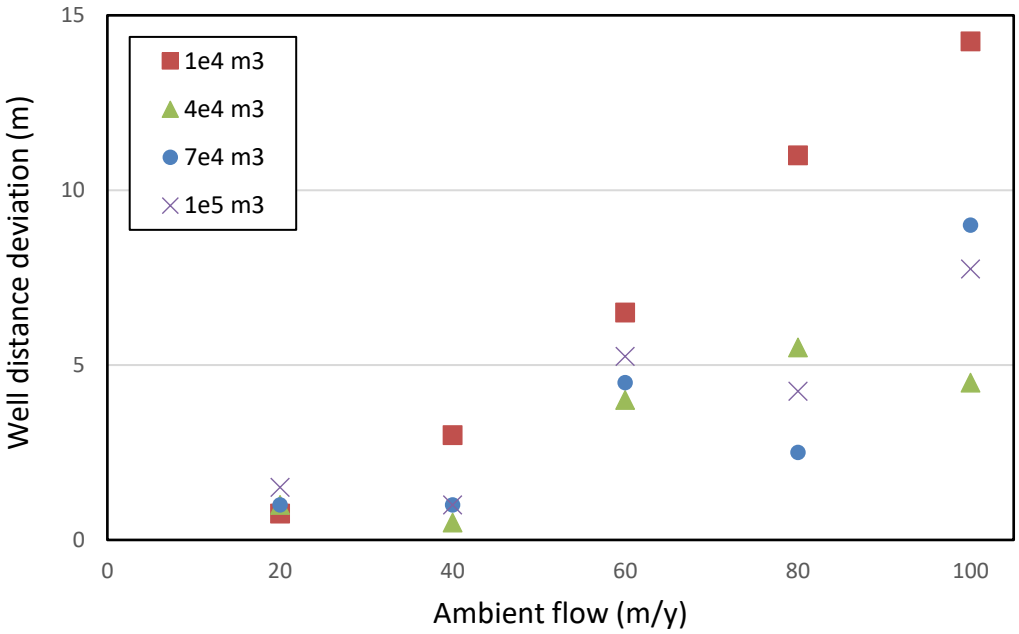

Figure 31. Difference in well distance for scenarios accidental and optimized scenario with an angle of 20 degrees between the wells and the flow field. Positive values indicate that the non-optimized well distance is larger.

Figure 32 describes the relation between the RE of the simulations in the base and dispersion scenarios against the RE when the wells are placed at an angle with the flow field. In the scenarios without ambient flow no deviations occur, as expected. With increasing ambient flow, the RE at 20 degrees (RE_{20}) decreases rapidly by 0.68 for an injection volume of 10 thousand m^3 and dispersion of 0.001. The optimized equivalent remains relatively stable and has a reduced RE of 0.11 (Figure 32). The impact of vertical hydraulic length is shown by the downward trend over volumes. At a dispersion of 0.5 m, the decrease in RE_{20} is 0.51 and 0.24 for injection volumes of 10 and 100 thousand m^3, respectively. Overall, the low dispersion scenarios show the highest sensitivity to the introduction of an angle.

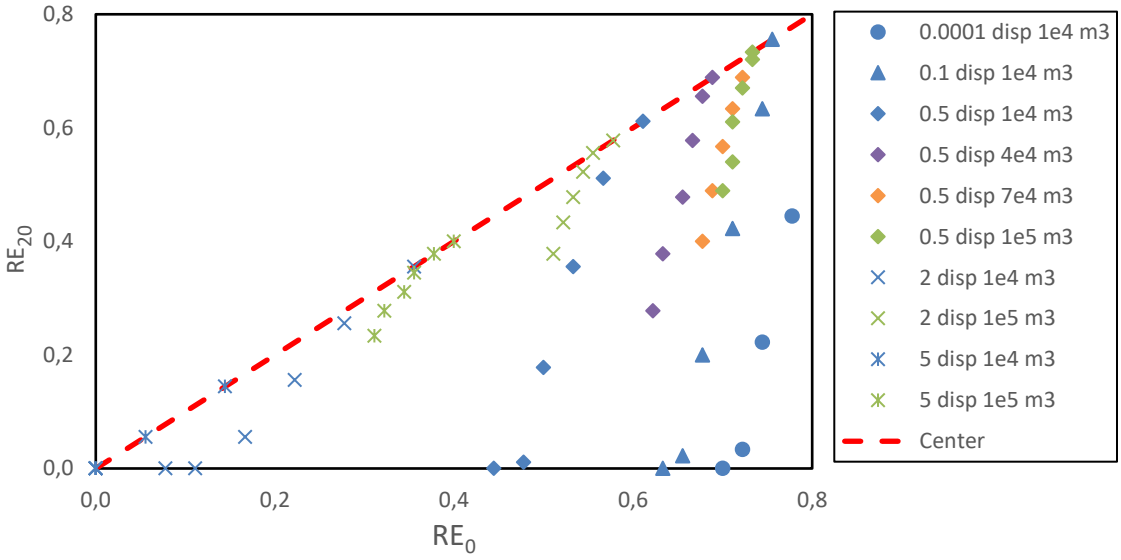

Figure 32. RE of the optimized scenarios against the RE with the same distance between the well, where β = 20 degrees.

5. Discussion

5.1 Decrease optimization time

The optimization of the well distance can be performed in multiple ways. In this study the model was initially calculating optimized well distances based on RE without prior knowledge. The performance was then evaluated based on graphs of the MF (Figure 33), RE, RE_{inj} and the concentration maps. With this approach only one well distance was run at the same time after which an analysis had to be performed to improve the well distance. Therefore, the automatization process by the iteration principle in Figure 5 was implemented. However, this steeply increased the runtime and created several scenarios which were not further used in this study. Therefore, the aim was to decrease runtime but conserve output quality.

After running the base scenario with the automated system, the optimized well distance was shown to be roughly estimated by the analytical approach. From that moment on, the model was converted to produce a starting value itself based on ambient flow, storage, and injection time. The reliability of the analytical approach was in all scenarios within 15 meters. This allowed the initial step size to decrease from 32 to 8 m, decreasing the number of unnecessary runs and the number of iterations before the step size was equal to cell size. As a result, runtimes were reduced by more than 60%.

The method to validate the model outcome by checking the concentration maps, clearly showed the lowest concentration spots where freshwater was not extracted in non-optimized simulations. Figure 34 shows the concentration map for a simulation from the base scenario of a non-optimized ASTR system. The remaining volume within the concentration line indicates the injection volume of sufficient quality that is not recovered. Herein lays a potentially more accurate method to find the optimum and decrease runtimes further. The center of the injected volume at the time where extraction starts can be found, by extracting concentration maps. This information combined with the prediction of injection and extraction shapes based on the time of travel parameter, may be a more efficient method to find the optimized well distance. If this process can be automized, it may be a powerful tool to find the optimized well position.

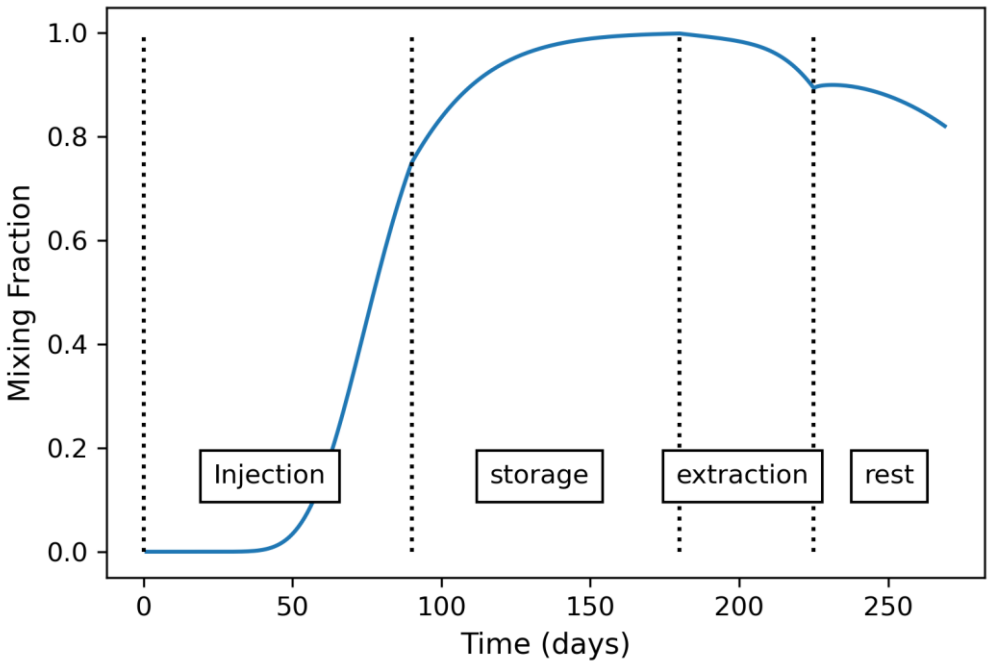

Figure 33. MF observed in the downstream extraction well at the optimized distance of 28.5 m, V_{amb}= 60 m/y and V_{inj} = 10 thousand m^3. After 45 days of extraction (day 225) the cutoff is reached and extraction is stopped.

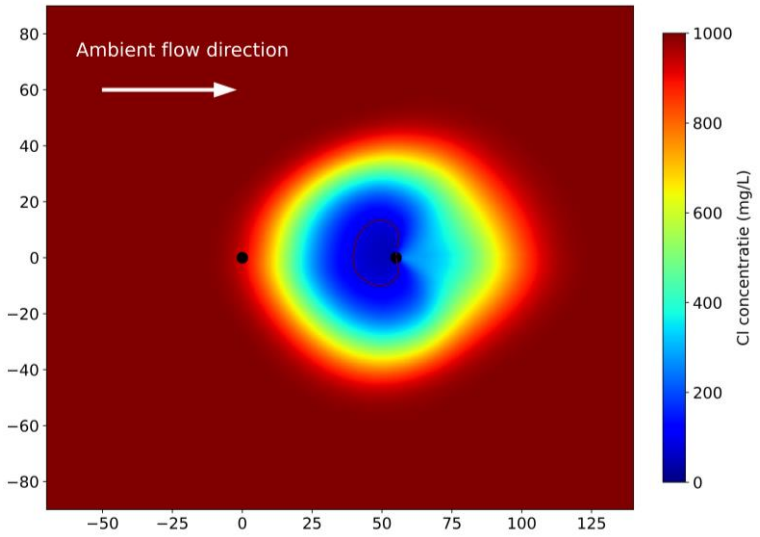

Figure 34. Concentration map of a non-optimized ASTR system with the extraction well at 40 m, V_{amb} = 100 m/y, V = 100 thousand m^3, α= 0.5 m. The black line indicates the extractable volume within the cutoff.

5.2 Optimized well location

Ideally, the optimized well distance calculated with EQ 10 gives a RE of 1 without dispersion and shape distortion due to ambient flow. In practice, dispersion induces mixing processes causing ambient water to enter the well quicker and decreasing the RE. Furthermore, the approach does not consider the deviating shape of the injection volume due to the non-instantaneous injection. Despite the optimized well location for the ASTR system showed high correlation with the analytical estimation for the location of the center of the freshwater volume at the beginning of extraction in most cases.

Some numerical scenarios result in deviating well positions from the analytical approach. Figure 13 and Figure 20 describe the deviations of the optimized well distance with respect to expected values based on EQ 10 for ambient flow, dispersion and injection volume. In this section, the validity of the analytical approach will be discussed for these parameters.

Performance of analytical approach

The estimation of the analytical approach showed deviations across several simulations in the dispersion and base scenario (Figure 13 and Figure 20). The RE of the corresponding analytical ASTR system, is however very similar to the optimized ASTR system (Figure 35). For a volume of 10 thousand m^3 and α ≥ 2 m, the analytical ASTR setup shows significantly lower RE's. However, for these cases the optimized ASTR systems result in a RE < 0.2, therefore, even these optimized ASTR systems are not likely to be put into practice.

The analytical approach may thus seem a reasonable estimation for an ASTR setup at the first sight. However, it should be noted that these systems are based on the RE rather than the RE_{inj}, which may give rise to some further deviations, decreasing the effectiveness of an analytical ASTR setup with respect to the optimized system. As for the comparison between ASR and analytical ASTR systems, the conclusions with respect to RE are similar as for optimized ASTR systems. At higher ambient flows and V_{amb}/R_h ratios > 2, the RE of the ASR setup decreases to 0, whereas for analytical ASTR systems the RE remains relatively stable.

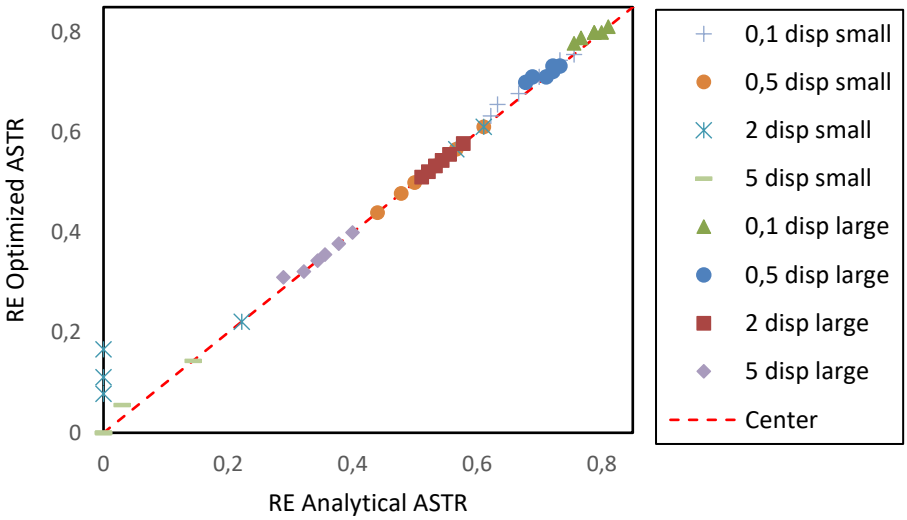

Figure 35. RE of ASTR systems at the optimized well distance against ASTR systems at the analytical well distance.

Deviations by cutoff and extraction period length

The capture zone is a mathematical approach to the water recovered from the subsurface, it does not consider the mixing effects and plume spreading. For pollution containment, this problem can be overcome by introducing a safety factor and increasing the pumping rate. In the case of AS(T)R for freshwater storage, the quality of the extraction water is leading. Whenever too saline water is recovered from the well, the extraction stops and all remaining freshwater is considered lost. This inherent feature of the system creates an extremely high pressure on solely extracting water of sufficient quality. The idea of a safety factor is reversed in this case. Without knowledge from numerical modelling, it is safer to create a capture zone, which is smaller than the injection volume to decrease intrusion of ambient water.

The analytical approach proposed in this thesis fails when RE at the optimum well distance is low. Figure 36 shows that the analytical approach increasingly overestimates the optimum well distance with decreasing RE. This approach assumes an extraction period of 45 days to find the optimized well position. But, when the optimized RE is very low, the movement of the injection volume during this short extraction period is limited. At an RE<0.2, the error in the assumption is such that the term $0.5*t_{ext}$ from EQ 10 decreases by a power of 3, hence the assumption of 45 days of extraction is invalid. When applying a refinement to incorporate the extraction time, the relative error in optimum well distance for low RE's decreases. In the case of an injection volume of 10 thousand m^3 with ambient flow of 100 m/y and a dispersion of 2 m, the RE is 0.08 and the optimized well distance is 38 m. Originally, the analytical estimation was 49 m, with the inclusion of the knowledge on the length of the extraction period (7 days), the optimized well distance is 38.9 m. This further deviation can be assigned to mixing effects.

As shown in the example above, the used analytical approach holds when considering the length of the extraction period. This parameter can only be determined by numerical modelling. As such the correction for the decreased extraction cannot improve the analytical approach without an underlying numerical model.

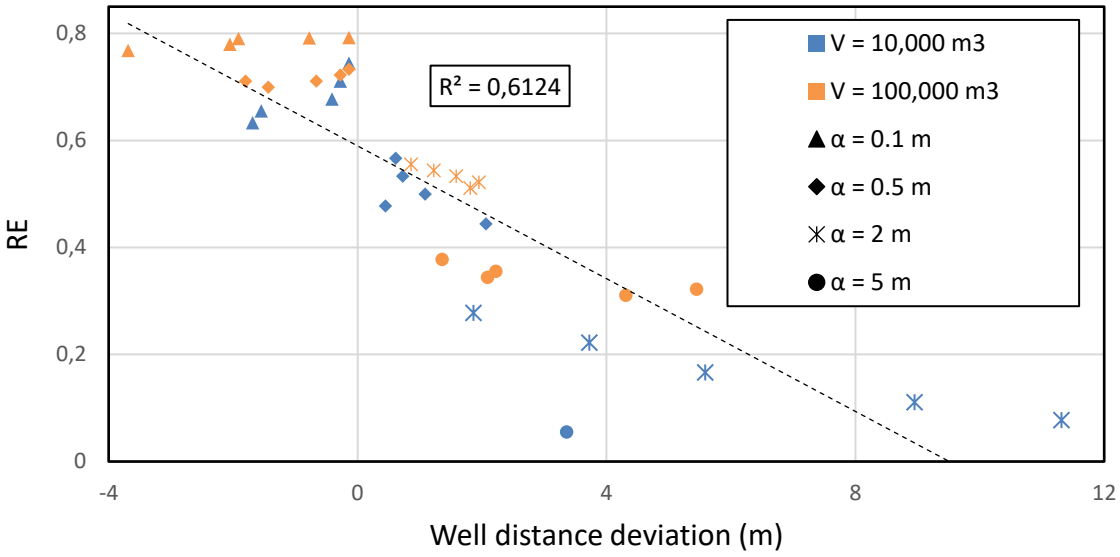

Figure 36. RE of the optimized ASTR systems against deviation of the optimum well distance from the analytical well distance for the dispersion and base scenarios. Positive deviations indicate that the analytical approach overestimates the optimum distance.

Deviations by edge effects

An extra factor that should be considered when determining the optimized well position are the edge effects. At the boundaries of the injected freshwater volume and ambient groundwater interface mixing will take place, due to diffusion and more importantly dispersion. Small volumes have a large interface to volume ratio with respect to the larger volumes. As a result, relatively more mixing takes place and RE decreases. The optimized well positioning is also affected by these edge effects. The radius of curvature of the injection volume is an indicator of the area surface ratio and determines the impact of combined effects from longitudinal and transverse dispersion (Figure 37). For circular volumes, the radius of curvature is large and the dispersed area is approximately circular as well. For the stadium shaped volumes, the tips with small radii of curvature have a large interface with ambient water and experience relatively high longitudinal and transverse dispersion. As a result, only the core of the injection volume contains water with a MF below the cutoff. This process moves the optimized well distance closer to the center of the injection volume and decreases the optimized well distance (Figure 20). Overall, the smaller volumes are likely to experience more deviation from the analytical well distance by edge effects due to their large edge to volume ratio.

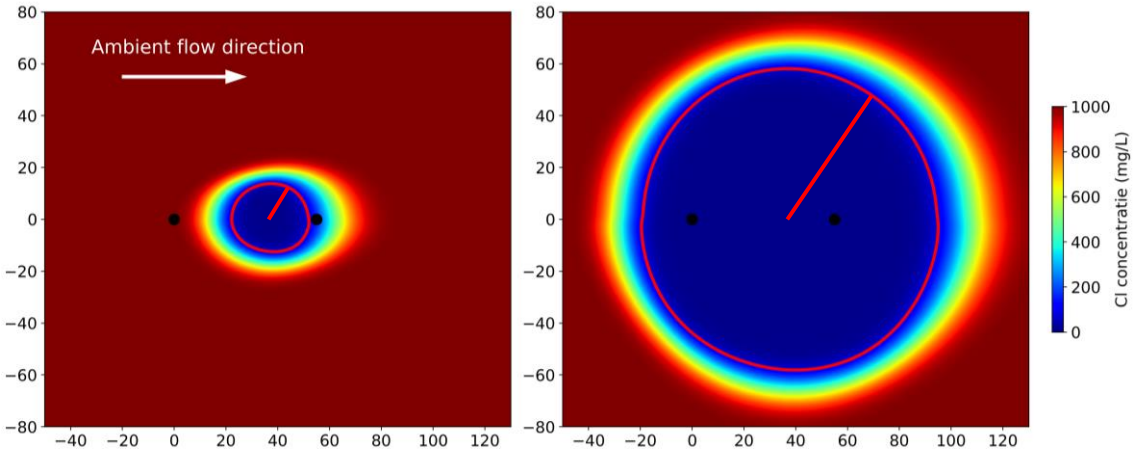

Figure 37. Radii of curvature of the injected freshwater volume above the cutoff at the end of the storage phase, where V_{inj}= 10 (left) and 100 (right) thousand m^3 and V_{amb}= 100 m/y.

Deviations by injection shapes and capture zones

τ values can be determined, based on the pumping rate, pumping timespan and ambient flow of each scenario. This parameter predicts the shape of the injection volume. The scenarios in this study result in a range of values for τ, listed in Table 6 and based on EQ 7. Without flow or for larger volumes with low ambient flow (< 40 m/y), the $\tau < 0.1$ (Table 6) resulting in circular injection and extraction volumes (Figure 42). For larger volumes at low ambient flow the $\tau<0.1$ and the instantaneous injection assumption holds, and the injection and extraction volumes are still circular. In other words, EQ 10 still holds. For small volumes and with high ambient flow, the injection volume is more ellipsoidal and cigar shaped (Figure 42). All other scenarios have $0.1<\tau<1$, resulting in an approximate circular injection volume, shifted downstream with respect to the injection well location (EQ 8).

At small dispersion, the injection volume stays compact and an ideal scenario where no mechanical dispersion occurs is approached, numerical dispersion remains present. As shown in the dispersion scenario, small dispersions lead to underestimations of the proposed analytical well distance. This is because, the approach in this study does not account for the change in capture zone, with changing τ value. While in practice, with increasing τ value, the optimized well location shifts downstream when ambient flow is introduced. In a scenario without mixing and no deformation of shape of the injection volume, the injection volume can be fully recovered even if ambient flow is increased, under the assumption that ambient flow is constant throughout the simulation.

Table 6. time-of-travel parameter τ, for different scenarios. Scenarios in green create symmetrical circular volumes around the well, in orange shifted circular volumes and in red stadium shaped volumes are injected.

Ambient flow (m/y)	Volume (10^3 m3/y)			
	10	40	70	100
0	0.00	0.00	0.00	0.00
20	0.11	0.03	0.02	0.01
40	0.43	0.11	0.06	0.04
60	0.96	0.24	0.14	0.10
80	1.71	0.43	0.24	0.17
100	2.67	0.67	0.38	0.27

Alternative analytical approach

EQ 10 is used as the analytical approach in this study. It estimates the distance travelled by the injection volume in the subsurface due to the ambient flow. This analytical estimation works well for simulations with a dispersion of 0.5 m, ambient flow conditions between 0 and 100 m/y and injection volumes between 10 and 100 thousand m^3. However, this estimation is not accurate for all conditions discussed in this study. This arises from a threefold problem. Firstly, within this simple approach it is hard to account for the complex edge effects, related to surface area and dispersion. This error is hard to quantify and is discussed in the paragraph Deviations by edge effects. Secondly, extraction is stopped immediately after water below the cutoff is extracted, the solution to this problem was discussed in the paragraph Deviations by cutoff and extraction period length, but only works in retro perspective. Thirdly, the τ is a parameter that induces deviations from circular injection shapes, decreasing the accuracy of the analytical approach.

Here, a method is proposed to account for the latter cause of deviations, changes in shape of the injection volume based on τ. The method is based on mathematical work from Ceric and Haitjema (2005). It may help understanding the deviations by ambient flow and injection rates.

For the simulations where $0.1<\tau<1$, the injection volume remains approximately circular, but the origin of the circle is not the location of the injection well. The volume will be shifted downstream by a factor δ during injection in comparison to a similar volume without flow (EQ 8) (Ceric & Haitjema, 2005). The optimized location of the extraction well will also be shifted downstream by this factor, resulting in a

total shift of 2δ. Over all scenarios where 0.1<τ<1 the shift is between 0.14 and 1.29 m, depending on ambient flow and injection volume.

When τ>1, the capture zone is ellipsoidal and cannot be approximated with a circular shape. The downstream length is equal to the distance to the stagnation point (L_s). The ratio of upstream length (L_u) and the length to L_s of captured volume is described by (Ceric & Haitjema, 2005):

$$N = \tau + \ln(\tau + 1) \qquad \text{EQ 18}$$

Where N is the ratio of L_u/L_s (-).

The stagnation point by Ceric and Haitjema (2005) is defined in relative coordinates, such that the extraction well is at x=0 and the stagnation point is at x = 1. The upstream length of the extracted volume is equal to N, making the length of the volume N+1. When converting these relative coordinates into absolute coordinates, total volume length is given by L_u+L_s. For injected volumes, the shape is inverted, as such $L_{d\text{-}ext} = L_{s\text{-}inj}$ and $L_{s\text{-}ext} = L_{d\text{-}inj}$.

At the end of the injection period, the most downstream part of the injection volume is located at x = $L_{d\text{-}inj}$. During the storage period the volume moves with a velocity of V_x for an extraction time of t_{ext}. At the end of extraction, capture zone should include the whole injection volume. The front of the plume is at the distance traveled during storage plus $L_{d\text{-}inj}$. The optimal location for the extraction well is now equal to the front of the plume minus $L_{d\text{-}ext}$ (or $L_{s\text{-}inj}$) (Figure 38). The ideal location for the extraction well thus undergoes a shift of $L_{d\text{-}inj}$-$L_{d\text{-}ext}$, or in relative coordinates N-1. The optimized well distance (L_{opt}) for all τ values becomes:

$$L_{OPT} = L_{d-inj} - L_{d-ext} + (t_{storage} + t_{ext})V_x$$

For τ<0.1, $L_{d\text{-}inj}$-$L_{d\text{-}ext}$ =0

For 0.1< τ<1, $L_{d\text{-}inj}$-$L_{d\text{-}ext}$ = 2δ

For τ>1, $L_{d\text{-}inj}$-$L_{d\text{-}ext}$ = (τ+ln(τ+1)-1)*L_s

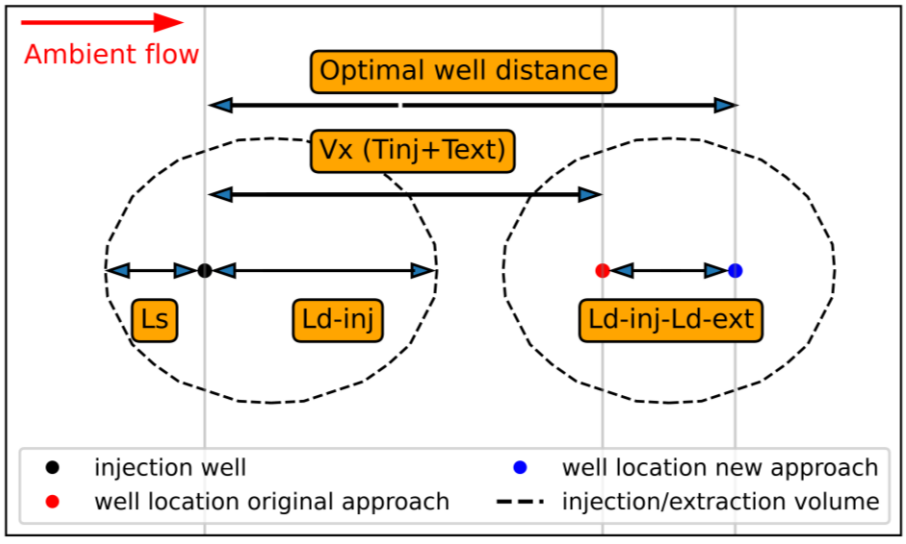

Figure 38. Alternative approach to find analytical expression for optimized well distance. Where the injection well is located at x=0 and the extraction well at the optimized distance (wd). L_s is the length to the stagnation point, L_{inj} is the downstream length of the injection volume.

When applying this new approach to the data, the analytical estimate of the well distance is increased for all cases where τ≥0.1. However, as described by Figure 13 and Figure 20, for α > 0.5 m the original analytical method already overestimated the optimum well distance for ASTR systems and will therefore not result in more accurate estimations. In the domain of α < 0.5 m, this new approach improves the

estimations of the optimum well distance. For example, for a volume of 10 thousand m^3 at α = 0.1 m, the optimum well distance is 30.5 m, the original analytical estimate was 29.5 m but with the new approach the estimate is 30.2. For a volume of 100 thousand m^3 and α < 0.5 m, the renewed analytical estimate is also improved, but only by a distance between 0.1 and 0.2 m.

Relevance of analytical approach

The renewed approach was not preferred in this study, because the deviations from the analytical well distance increased in most cases by implementing this adjustment, only for $\alpha \leq 0.1$m the renewed approach resulted in better approximations. Furthermore, the purpose of the applied analytical estimation in this study was only to reduce runtimes of the model. It did not attempt to reflect the complex reality in the subsurface. The applied analytical estimation slightly underestimates the optimized well distance by assuming circular volumes and instantaneous injection. However, the edge effects decrease the optimized well distance, but are unaccounted for in both the applied and proposed approach. This is a possible explanantion as to why the applied method may have fitted the data better, eventhough the hydrogeological substantiation is less accurate.

As discussed earlier (5.1 Decrease optimization time), the analytical approach is a tool to rougly estimate the optimized well location. This decreases runtimes drastically. However, the analytical approach is not linked to the overall RE of the ASR and ASTR system. This can only be determined by using numerical modelling. Therefore, the necessity of a highly reliable analytical approach is low in this study. For future modelling and in practice application of the analytical well distance, it may be desirable to have a more accurate approach. The key variable to grasp in later studies, is the displacement of the optimized well location due to mixing effects.

5.3 Modelling obstacles

The creation of the hydrogeological model spanned a large part of this thesis. Several problems were encountered during the development and validation phase, most of which were solved. However, two of these irregularities were not entirely resolved, one in the chemical transport and another in the hydraulic heads.

Steady state modelling

The boundaries of the model are located far from the region where chloride transport occurs. The initial hydraulic head of the model was set at the value of the lowest boundary (50 m) in all cells, except for the constant hydraulic head boundary on the left. During transient modelling of the hydraulic head, the equilibrating of the in all cells at the start of the simulation resulted in a delay of the observed ambient flow. The model showed no flow for several days, decreasing the optimized well distance and alternating the RE. To solve this problem, a steady state model was run for the hydraulic head. However, as steady state did not seem to have an effect, the runtime of the pre-model was chosen such that the head contours were established and remained stationary. In this way, a workaround for this issue was developed. For the larger models, this process is time costly. But preparing head conditions before the run is believed to be an essential step to generate valid results. Another possibility to create a starting gradient in the model grid is by assigning the values to the initial grids. However, the use of a nested grid complicates this, as the cells are not aligned per column as is the case for a regular structured grid.

Irregularity

The model contains an irregularity in the transport region, which became visible at high dispersivity values (Figure 40), for lower dispersivity values the anomality was less evident. In the line y = 0 the model should be symmetrical for the cases without angle. However, according to Figure 40A and B this is not the case for high dispersivity values with small volumes. In Figure 18, the deviation is also visible for the optimization curve of the no ambient flow scenario. It is expected to be symmetrical around x=0, but instead, the optimized well distance is found at x=-1.

This irregularity occurred only during the injection phase. Upon movement of the waterbody in the storage phase, the concentration contours smoothened and the effect of a supposed constant

concentration cell faded (Figure 40A and B). No constant concentration cells were found to have caused this behavior. Furthermore, head contours showed no deviations during the injection period (Figure 9 and Figure 39). For the large volume in Figure 40C, another irregularity occurs in plane y = 0, which is likely caused by the same error. From this figure it becomes clear that a constant concentration cell is not likely to be the cause of the problem, since the injection volume does not have an equal steep concentration gradient as the smaller volume. Another reason to rule out the presence of the constant concentration cell was established by mirroring the ambient flow of the model in x = 50. The head boundaries were placed such that ambient flow was from right to left and the injection well was moved towards the right boundary. This resulted in the same asymmetry in the model. Potential influence of the change in signs at the origin of the model, where the injection well is located, was ruled out by running the model in a coordinate system with only positive values. This model encountered the same issues with the dispersivity. A possible explanation for the irregularity is a numerical error due to the application of the nested grid. Unfortunately, this could not be confirmed and solved. Therefore, at high dispersivity values the model is likely to have some error in the absolute RE's.

However, all scenarios without an angle have the injection and extraction well placed on the line y = 0, the same line as where the irregularity occurs. Since this anomality is present in all runs, it is possible to look at the RE from a relative perspective. Furthermore, most non-symmetrical scenarios were run with a lower dispersivity value, where less visible deviations were present. This supports the belief that absolute RE's of these scenarios are less influenced by the irregularity and thus more accurate.

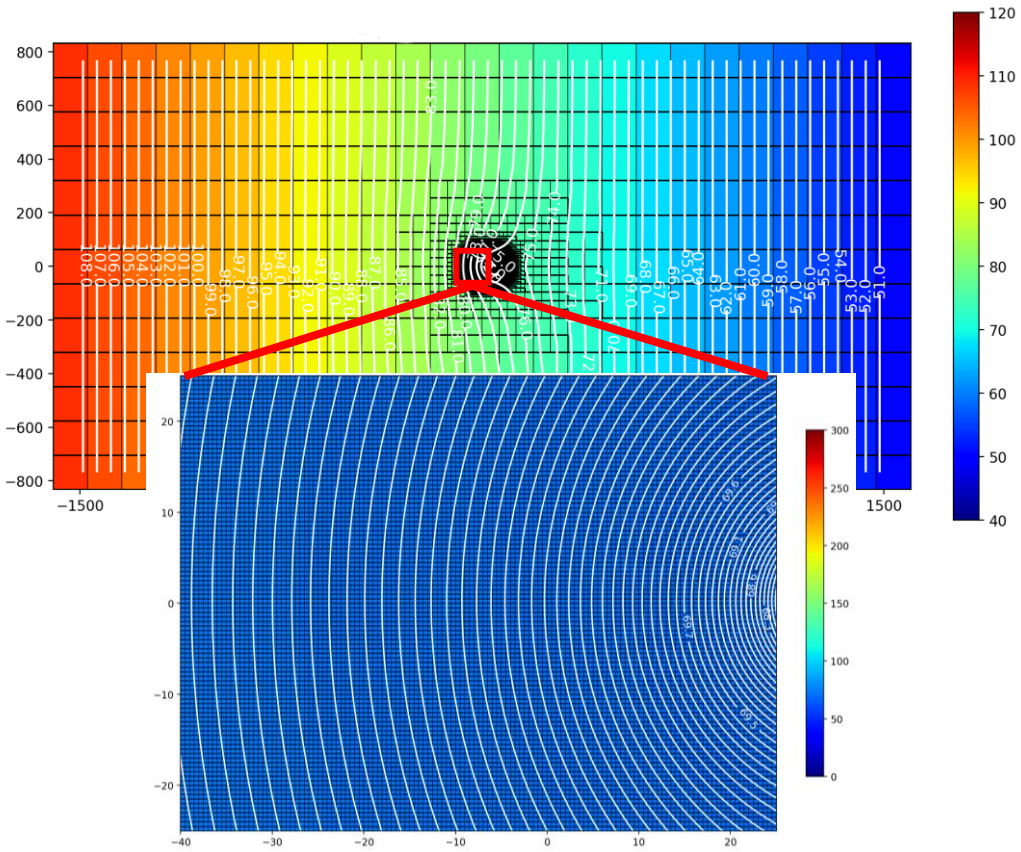

Figure 39. Head contours for the injection period for the whole model and located slightly upstream of the injection well.

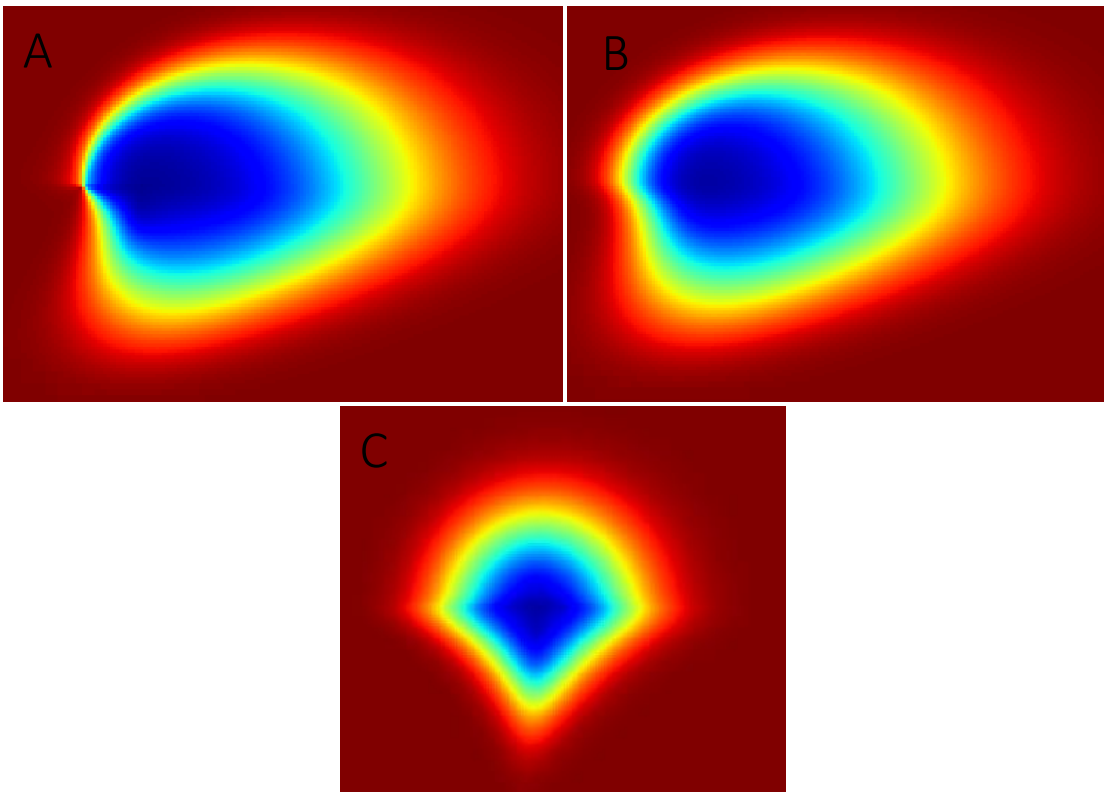

Figure 40. Asymmetrical irregularities in the injected volume where α_L=0.5 m , for a small volume during injection (A) and storage (B) and for injection of a large volume (C).

5.4 Multicyclic simulations

Some ASR applications have an increased performance over the years (van Ginkel et al., 2014). Due to the dispersion and 0.9 MF cutoff, part of the injected volume is not recovered during the extraction phase. The mixed water remaining in the aquifer creates a less saline environment for the next injection cycle. This decreases the impact of mixing on the newly injected volume and can result in an extraction volume gain equal to 50% of the injected volume (van Ginkel et al., 2014). This is only valid for aquifers without or with little ambient flow. Before a new cycle is started, the waterbody remains intact and is only affected by molecular diffusion. However, when ambient flow is present, as in this study, the remaining freshwater flows through the aquifer away from the extraction well and mixes with ambient water. At low ambient flows, some remaining freshwater may be present at the extraction well during the new cycle, depending on the injection volume, hydraulic radius, and ambient flow. The remaining volume is expected to have an impact on the multiyear RE for cases where:

$$V_{amb} * t_{cycle} < R_h \qquad \text{EQ 19}$$

with t_{cycle} is the time between cycles and R_h is the hydraulic radius of the initial injection volume.

When EQ 19 does not hold, recovery in a new cycle is not possible due to the lateral movement of the injected volume. These cases are described by high ambient velocities and long timespans between cycles. The dispersion is a factor that complicates estimation for the potential of multicyclic ASTR systems. On the one hand, the area of the injected freshwater volume expands due to dispersion and Brownian motion. On the other hand, the remaining low concentration volume increases in concentration and so the concentration gradient in a new cycle becomes larger. This decreases the benefit for multicyclic systems. In general, multiyear simulations and field applications are not expected to have a substantial impact on RE over cycles under ambient flow conditions, except when $V_{amb}*t_{cycle}<<R_h$.

5.5 Cutoff

The cutoff for acceptable extraction water determines the RE. At the first observation of extraction water below the quality standard, extraction is terminated and all remaining freshwater is considered lost to the environment. In this study, a strict cutoff is used to recover volumes at drinking water quality. Figure 8, Figure 10 and Figure 19 show that relatively fresh water remains around the well after the cutoff is reached. Performance of these ASR and ASTR systems may be improved by distinguishing between purposes of the extracted water. The initially recovered high quality water can be used for the most sensitive purposes as drinking water, whereas more saline water can flow to industrial processes.

The cutoff is an indicator of the relative MF. The chosen injection and ambient concentration of 10 and 1000 mg/L are not the only scenarios described by this model. For any injection concentration with the same relative difference with ambient concentration (ratio 0.01), these results will be reproduced. During the validation stage of this model, a ratio of 0.08 (80 over 1000 mg/L) was used for the injected and ambient water. The cutoff was defined at 150 mg/L, allowing only 7.7% mixing. The combined effect of increased concentration ratio and stricter cutoff decreased RE between 0.05 and 0.1 for simulations within the base scenario (Figure 41). In this study, only a small range of ratios was covered. Globally, the salinity of aquifers is highly variable, with typical chloride concentrations between 0.4 and 40 g/L (Van Weert et al., 2009). As a result, ratios can vary by a factor of 40 solely based on ambient concentrations. This indicates that the concentration ratio of the aquifer is an important parameter that needs to be evaluated before planning AS(T)R systems to assess the magnitude of mixing effects.

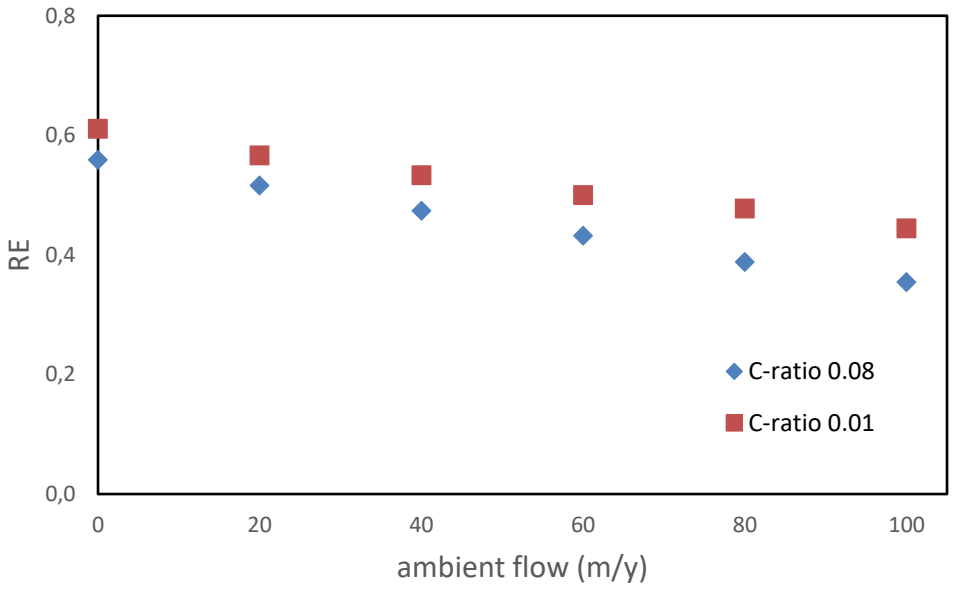

Figure 41. Performance of the optimized ASTR system for different injection and ambient concentration ratios where α_L=0.5 m.

5.6 Practical implications

Operation policy

The operation policy of both injection and extraction well can be of influence on the RE. Throughout this study the injection and extraction time were constant. Furthermore, extraction time and rate were set at the same values as the injection parameters.

The cutoff concentration in the well was reached in all scenarios by intrusion of ambient water either upstream or downstream of the well, except for the no flow scenarios, which were symmetrical in both x- and y-direction. In a scenario with a prolonged injection phase of 180 days the injection volume was more cigar shaped. During the 90-day extraction phase, a twice as high pumping rate was applied. This resulted in intrusion of ambient water perpendicular to the flow direction. This supports the idea that

the injection rate is a limiting factor for the extraction rate and should ideally be similar when injection and extraction phases are equally long.

For simulations in this study, extraction with the same pumping rate is expected to result in the high recovery volumes. However, for future studies, if the injection time is long and the injection rate is relatively small, a more cigar shaped volume is created. In an aquifer with high dispersion in the transverse direction, an even thinner cigar shaped volume will remain suitable for extraction. In such an extreme case it may be preferred to decrease the extraction rate, to minimize perpendicular intrusion of saltwater.

Another factor potentially decreasing the RE are inconstant injection rates. Water availability may not be consistent over the whole injection period, leading to variations in the injection rate. This will create less symmetrical injection volumes with increased interface to volume ratios. As we have shown for small and large volumes, the increase in this ratio leads to more mixing and a decrease in RE.

This study presented impressive potential for ASTR systems when the operation policy is predictable and constant. Nevertheless, when the operation policy is not constant, this introduces new variables. These variables potentially affect the optimized well positioning. Therefore, it may be useful to explore the impact of the operation policy on the RE, before applying this technique in the field.

Uncertainties ambient flow

In the field, subsurface parameters are not always well defined. Uncertainties in or lack of measurements can result in inaccurate input parameters. The two uncertainties that are evaluated in this study are the magnitude of the ambient flow and the angle between the flow field and the plane of the injection and extraction well. For ASR systems, these have no other effect than a change in the RE. For ASTR systems, the optimized well positioning is affected by these uncertainties. In this section, the sensitivity of ASTR systems to these deviations are evaluated.

Magnitude

Inaccuracies in or absence of field measurements can introduce deviations between the expected and actual field magnitude of the ambient flow. This induces an inevitable error in the optimized well distance for the ASTR system. The optimization curves in Figure 12 and Figure 18 describe the dependency of RE on well distance. Due to the temporal discretization, different well positions were found with similar RE's (Figure 12 and Figure 18). For smaller systems, the optimized well distance remains stable in a range of 0.5 and 2.5 m for both the base scenario and higher dispersion scenarios. Larger systems are slightly less sensitive with stable RE in distances over 2-4 m. In the current temporal scale, ambient flow is affecting the lateral movement over 180 days according to the analytical approach. This means that for this numerical approach, the RE can remain constant at uncertainties in the ambient velocity of 0.25-1.5 m/y. However, this uncertainty factor in the can be 10x larger (Bakx et al., 2019; Coluccio et al., 2021; Reimus & Arnold, 2017).

With overestimations in the magnitude of the ambient flow of 15 m/y, RE drops are between 20 and 50% of the total RE for a volume of 10 thousand m^3 at an expected ambient flow between 0 and 100 m/y. For underestimations of the ambient flow, the RE decreases by 50-100%. For larger volumes, this sensitivity is lower with relative losses in RE of 6-15% for overestimations and 8-20% for underestimations. Underestimations of the ambient flow seem more impactful on RE, which can be explained by the stop of extraction when the cutoff is exceeded.

The deviations in ambient velocity can decrease the RE of the ASTR system. But this drop may not be inevitable. By increasing or decreasing the storage time, the fluctuations in ambient flow can be controlled. Especially over multiple cycles, this tradeoff can be optimized in practice.

Angle

In practice, well placement may be limited by the conditions at the surface. Due to construction and protected areas for example, the injection and extraction wells may not be constructed entirely in line

with the ambient flow. For ASR, angular dependency does not affect the RE due to the combined injection and extraction function of the well. For ASTR however, the separation of the wells introduces an angular dependency. Figure 30 and Figure 32 have shown that the RE of systems at an angle decrease even for an optimized scenario.

In this study, the angle between the flow field and the wells was up to 20 degrees. This resulted already in large decreases in RE, especially for small volumes. In practice, the uncertainty in the direction of the flow field can reach 45 degrees, due to the expression of the flow direction by cardinal direction in the compass. This will likely decrease the RE of the optimized ASTR system further, with respect to an ASTR system without angle. Therefore, the risk of implementing ASTR systems without profound knowledge on the flow conditions in the subsurface is very large and can potentially result in a very poorly performing system.

5.7. Prospects

This model, like any other, represents a simplified version of reality. This model is one-layered and homogeneous. As this study does not represent a specific site, input parameters are chosen based on common values in literature (Bloemendal & Hartog, 2018; Bloemendal & Olsthoorn, 2018; Culkin et al., 2008; Sallam, 2019; Ward et al., 2008). However, this model has high potential for differentiation in different environments. By extending with multiple layers, the 2D concepts can be studied in 3D. By introducing heterogeneity, the density effects can be assessed.

Ambient flow can be altered, to account for uncertainties in the field application. The angular dependency of the well placement with respect to the direction of the ambient flow can be easily simulated. This can give a fast insight into the optimized RE of an ASR or ASTR system at a given location as well as the risks related to the uncertainties. Due to its flexible nested grid, the refined area can be adapted to any given shape. Therefore, the range of volumes suitable for the model is wide, without increasing the runtime of simulations unnecessarily. The flexibility in the injection, storage and extraction times generate scenarios on a temporal resolution of 1 day.

This study and the underlying model can serve as a tool to explore the feasibility of a subsurface freshwater storage system. It gives insight into the necessity of a separate injection and extraction well. Furthermore, the future model outcomes may support discussion on operation policy. With small modifications the model will also be suitable for multilayer simulations as well as a heterogeneous subsurface. At the cost of runtime, this can increase the accuracy and applicability of the model to case studies and establish the effect of buoyancy.

6. Summary and conclusion

In this study, the numerical modelling of aquifer storage, transfer, and recovery (ASTR) and aquifer, storage and recovery (ASR) systems showed the impact of ambient flow, dispersion, injection volume and uncertainty in flow parameters on the recovery efficiency (RE) and optimum well distance.

At a ratio of ambient flow over hydraulic radius >2.5 the RE of the ASR system decreased to 0. The optimized ASTR systems in contrast, showed a relative gain in RE with respect to the ASR systems between 0.7 and 0.44 for V_{amb}/R_h ratios up to 4.7 and $\alpha \leq 0.5$ m .

Increasing ambient flow up to 100 m/y showed inevitable decreases in RE, arising from mixing processes. At the interface of the injection volume, freshwater mixes with ambient water, due to hydrodynamic dispersion, decreasing the recoverable injected water volume. At higher ambient flows, the differences in encountered path lengths increase and the plume spreads out. Losses in RE of 0.03 to 0.6 were found, depending on the magnitude of the ambient flow and dispersion.

The hydraulic radius of the injection volumes determines the sensitivity to the other parameters. A high interface to volume ratio increases vulnerability of the injection volume to deformation due to ambient flow. Instead of a circle, the small injection volumes under high ambient flow become ellipsoidal, decreasing the volume to surface ratio further. Injection volumes of 10 thousand m^3 and V_{amb}>20 m/y were enough to decrease the RE to 0 at a dispersion of 5 m.

An analysis of the uncertainty in angle and magnitude of the flow field showed the importance of profound knowledge of the subsurface when implementing ASTR systems. ASTR systems showed constant RE with well distances deviating up to 4 m from the optimized well distance. Outside these domains, the RE drops, fast for small and moderately for larger injection volumes.

Volumes with small hydraulic radii are highly impacted by the introduction of an angle between the flow field and the wells. At high ambient velocities numerical simulations show a steep decrease in RE up to 0.41 at an angle of 20 degrees. Injection of larger volumes reduces the impact of the angle and allows for recovery of over 50% of the initial injected volume.

The change in RE for ASR and optimized ASTR systems is determined by separately studying the impact of transport processes. In summary, the following conclusions are made:

- When ambient flow is present optimized ASTR systems show higher RE's than ASR systems in numerical simulations.
- High ambient flow and dispersion decrease the optimized performance of ASTR systems
- Larger injection volumes reduce edge effects and increase RE at the optimized well distance for ASTR systems
- Uncertainty in the angle and magnitude of the flow field drastically decreases the RE of optimized ASTR systems.
- ASTR systems are potentially powerful systems to increase RE in regions with ambient flow. Their success is, however, highly dependent on the accurate determination of subsurface parameters, such as direction and magnitude of ambient flow.

This numerical model for ASR and ASTR systems provided the opportunity to compare the potential of ASR and ASTR systems. The flexible nested grid allowed for optimized runtimes depending on injection volume and ambient flow. The effect of individual transport processes on the RE and optimized well positioning was assessed. Analytical approaches to the optimized well distance were validated. Future improvements could make the model suitable for multilayer (3D) and heterogeneity simulations to assess buoyancy effects on ASTR systems in a flow field.

References

Bakker, M., Post, V., Langevin, C. D., Hughes, J. D., White, J. T., Starn, J. J., & Fienen, M. N. (2016). Scripting MODFLOW Model Development Using Python and FloPy. *Groundwater*, *54*(5), 733-739. https://doi.org/https://doi.org/10.1111/gwat.12413

Bakx, Doornenbal, Weesep, Bense, Essink, & Bierkens. (2019). Determining the Relation between Groundwater Flow Velocities and Measured Temperature Differences Using Active Heating-Distributed Temperature Sensing. *Water*, *11*(8), 1619. https://doi.org/10.3390/w11081619

Bear, J. (1972). *Dynamics of fluids in porous media*. Courier Corporation.

Bear, J., & Jacobs, M. (1965). On the movement of water bodies injected into aquifers. *Journal of Hydrology*, *3*(1), 37-57. https://doi.org/https://doi.org/10.1016/0022-1694(65)90065-X

Bloemendal, M., & Hartog, N. (2018). Analysis of the impact of storage conditions on the thermal recovery efficiency of low-temperature ATES systems. *Geothermics*, *71*, 306-319. https://doi.org/https://doi.org/10.1016/j.geothermics.2017.10.009

Bloemendal, M., & Olsthoorn, T. (2018). ATES systems in aquifers with high ambient groundwater flow velocity. *Geothermics*, *75*, 81-92. https://doi.org/https://doi.org/10.1016/j.geothermics.2018.04.005

Bloetscher, F., Sham, C. H., Danko Iii, J. J., & Ratick, S. (2014). Lessons Learned from Aquifer Storage and Recovery (ASR) Systems in the United States. *Journal of Water Resource and Protection*, *06*(17), 1603-1629. https://doi.org/10.4236/jwarp.2014.617146

Boretti, A., & Rosa, L. (2019). Reassessing the projections of the World Water Development Report. *npj Clean Water*, *2*(1). https://doi.org/10.1038/s41545-019-0039-9

Boumaiza, L., Walter, J., Chesnaux, R., Stotler, R. L., Wen, T., Johannesson, K. H., Brindha, K., & Huneau, F. (2022). Chloride-salinity as indicator of the chemical composition of groundwater: empirical predictive model based on aquifers in Southern Quebec, Canada. *Environmental Science and Pollution Research*, *29*(39), 59414-59432. https://doi.org/10.1007/s11356-022-19854-z

Bouwer, H. (2002). Artificial recharge of groundwater: hydrogeology and engineering. *Hydrogeology Journal*, *10*(1), 121-142. https://doi.org/10.1007/s10040-001-0182-4

Ceric, A., & Haitjema, H. (2005). On using simple time-of-travel capture zone delineation methods. *Groundwater*, *43*(3), 408-412. https://doi.org/https://doi.org/10.1111/j.1745-6584.2005.0035.x

Coluccio, K. M., Santos, I. R., Jeffrey, L. C., & Morgan, L. K. (2021). Groundwater discharge rates and uncertainties in a coastal lagoon using a radon mass balance. *Journal of Hydrology*, *598*, 126436. https://doi.org/https://doi.org/10.1016/j.jhydrol.2021.126436

Culkin, S. L., Singha, K., & Day-Lewis, F. D. (2008). Implications of Rate-Limited Mass Transfer for Aquifer Storage and Recovery. *Groundwater*, *46*(4), 591-605. https://doi.org/https://doi.org/10.1111/j.1745-6584.2008.00435.x

Dettinger, M., Udall, B., & Georgakakos, A. (2015). Western water and climate change [https://doi.org/10.1890/15-0938.1]. *Ecological Applications*, *25*(8), 2069-2093. https://doi.org/https://doi.org/10.1890/15-0938.1

Hajek, O. L., & Knapp, A. K. (2022). Shifting seasonal patterns of water availability: ecosystem responses to an unappreciated dimension of climate change [https://doi.org/10.1111/nph.17728]. *New Phytologist*, *233*(1), 119-125. https://doi.org/https://doi.org/10.1111/nph.17728

Intergovernmental Panel on Climate, C. (2022). *The Ocean and Cryosphere in a Changing Climate: Special Report of the Intergovernmental Panel on Climate Change*. Cambridge University Press. https://doi.org/DOI: 10.1017/9781009157964

Langevin, C. D., Hughes, J. D., Provost, A. M., Russcher, M. J., Niswonger, R. G., Panday, S., Merrick, D., Morway, E. D., Reno, M. J., Bonelli, W. P., & Banta, E. R. (2022). *MODFLOW 6 Modular Hydrologic Model version 6.4.1*. In (Version 6.4.1) U.S. Geological Survey Software Release. https://www.usgs.gov/software/modflow-6-usgs-modular-hydrologic-model

Liu, J., Fu, Z., & Liu, W. (2023). Impacts of precipitation variations on agricultural water scarcity under historical and future climate change. *Journal of Hydrology*, *617*, 128999. https://doi.org/https://doi.org/10.1016/j.jhydrol.2022.128999

Miotliński, K., Dillon, P. J., Pavelic, P., Barry, K., & Kremer, S. (2014). Recovery of Injected Freshwater from a Brackish Aquifer with a Multiwell System. *Groundwater*, *52*(4), 495-502. https://doi.org/https://doi.org/10.1111/gwat.12089

Neuman, S. P. (1977). Theoretical derivation of Darcy's law. *Acta Mechanica*, *25*(3), 153-170. https://doi.org/10.1007/BF01376989

Page, D., Bekele, E., Vanderzalm, J., & Sidhu, J. (2018). Managed Aquifer Recharge (MAR) in Sustainable Urban Water Management. *Water*, *10*(3), 239. https://doi.org/10.3390/w10030239

PWN. (2022). *PWN verkent ondergrondse waterberging als oplossing voor toenemende (piek)watervraag*. PWN. Retrieved 17-8-2023 from

Rasmussen, P., Sonnenborg, T. O., Goncear, G., & Hinsby, K. (2013). Assessing impacts of climate change, sea level rise, and drainage canals on saltwater intrusion to coastal aquifer. *Hydrology and Earth System Sciences*, *17*(1), 421-443. https://doi.org/10.5194/hess-17-421-2013

Reimus, P. W., & Arnold, B. W. (2017). Evaluation of multiple tracer methods to estimate low groundwater flow velocities. *Journal of Contaminant Hydrology*, *199*, 1-13. https://doi.org/10.1016/j.jconhyd.2017.02.003

Rijksoverheid. (2015). *Protocol voor monitoring en toetsing drinkwaterbronnen KRW*.

Rinck-Pfeiffer, S., Ragusa, S., Sztajnbok, P., & Vandevelde, T. (2000). Interrelationships between biological, chemical, and physical processes as an analog to clogging in aquifer storage and recovery (ASR) wells. *Water Research*, *34*(7), 2110-2118. https://doi.org/https://doi.org/10.1016/S0043-1354(99)00356-5

Ringleb, J., Sallwey, J., & Stefan, C. (2016). Assessment of Managed Aquifer Recharge through Modeling—A Review. *Water*, *8*(12), 579. https://doi.org/10.3390/w8120579

Sallam, O. M. (2019). Use of Numerical Groundwater Modeling to Assess the Feasibility of Aquifer Storage and Recovery (ASR) in the Wadi Watir Delta, Sinai, Egypt. *Journal of Water Resource and Protection*.

Scanlon, B. R., Fakhreddine, S., Rateb, A., de Graaf, I., Famiglietti, J., Gleeson, T., Grafton, R. Q., Jobbagy, E., Kebede, S., Kolusu, S. R., Konikow, L. F., Long, D., Mekonnen, M., Schmied, H. M., Mukherjee, A., MacDonald, A., Reedy, R. C., Shamsudduha, M., Simmons, C. T., . . . Zheng, C. (2023). Author Correction: Global water resources and the role of groundwater in a resilient water future. *Nature Reviews Earth & Environment*, *4*(5), 351-351. https://doi.org/10.1038/s43017-023-00418-9

Theis, C. V. (1935). The relation between the lowering of the Piezometric surface and the rate and duration of discharge of a well using ground-water storage. *Transactions, American Geophysical Union*, *16*(2), 519. https://doi.org/10.1029/tr016i002p00519

van Ginkel, M., Olsthoorn, T. N., & Bakker, M. (2014). A New Operational Paradigm for Small-Scale ASR in Saline Aquifers [https://doi.org/10.1111/gwat.12113]. *Groundwater*, *52*(5), 685-693. https://doi.org/https://doi.org/10.1111/gwat.12113

Van Weert, F., Van der Gun, J., & Reckman, J. (2009). Global overview of saline groundwater occurrence and genesis. *International Groundwater Resources Assessment Centre*.

Wang, X. S., Chen, C. X., & Jiao, J. J. (2004). Modified Theis equation by considering the bending effect of the confining unit. *Advances in Water Resources*, *27*(10), 981-990. https://doi.org/https://doi.org/10.1016/j.advwatres.2004.08.007

Ward, J. D., Simmons, C. T., & Dillon, P. J. (2007). A theoretical analysis of mixed convection in aquifer storage and recovery: How important are density effects? *Journal of Hydrology*, *343*(3), 169-186. https://doi.org/https://doi.org/10.1016/j.jhydrol.2007.06.011

Ward, J. D., Simmons, C. T., & Dillon, P. J. (2008). Variable-density modelling of multiple-cycle aquifer storage and recovery (ASR): Importance of anisotropy and layered heterogeneity in brackish aquifers. *Journal of Hydrology*, *356*(1), 93-105. https://doi.org/https://doi.org/10.1016/j.jhydrol.2008.04.012

Ward, J. D., Simmons, C. T., Dillon, P. J., & Pavelic, P. (2009). Integrated assessment of lateral flow, density effects and dispersion in aquifer storage and recovery. *Journal of Hydrology*, *370*(1), 83-99. https://doi.org/https://doi.org/10.1016/j.jhydrol.2009.02.055

Weissmann, G. S., Zhang, Y., LaBolle, E. M., & Fogg, G. E. (2002). Dispersion of groundwater age in an alluvial aquifer system [https://doi.org/10.1029/2001WR000907]. *Water Resources Research*, *38*(10), 16-11-16-13. https://doi.org/https://doi.org/10.1029/2001WR000907

WHO. (2003). Chloride in Drinking-water. *Guidelines for drinking-water quality*, *2*(2).

Zuurbier, K. G., Hartog, N., Valstar, J., Post, V. E. A., & van Breukelen, B. M. (2013). The impact of low-temperature seasonal aquifer thermal energy storage (SATES) systems on chlorinated solvent contaminated groundwater: Modeling of spreading and degradation. *Journal of Contaminant Hydrology*, *147*, 1-13. https://doi.org/https://doi.org/10.1016/j.jconhyd.2013.01.002

Zuurbier, K. G., Janmaat, P., Raat, K. J., Ros, S., & ter Mors, G. (2017). Waterhergebruik en -berging met aquifer storage and recovery (ASR) op tuinbouwlocatie Nieuw-Prinsenland. *H2O-Online*.

Zuurbier, K. G., & Stuyfzand, P. J. (2017). Consequences and mitigation of saltwater intrusion induced by short-circuiting during aquifer storage and recovery in a coastal subsurface. *Hydrology and Earth System Sciences*, *21*(2), 1173-1188. https://doi.org/10.5194/hess-21-1173-2017

Zuurbier, K. G., Zaadnoordijk, W. J., & Stuyfzand, P. J. (2014). How multiple partially penetrating wells improve the freshwater recovery of coastal aquifer storage and recovery (ASR) systems: A field and modeling study. *Journal of Hydrology*, *509*, 430-441. https://doi.org/https://doi.org/10.1016/j.jhydrol.2013.11.057

Appendix A

Table 7. Overview of the input parameters of the MODFLOW 6 model.

Parameter	Symbol	Value
Length (m)	Lx	3200
Width (m)	Ly	1664
Thickness (m)	D	20
Number of layers	nlay	1
Outer grid cell size (m)	Delc/Delr	128
Inner grid cell size (m)	Delc/Delr	0.25-0.5
Horizontal hydraulic conductivity (m/d)	Kh	5
Ambient flow (m/d)	Vamb	0-100
Longitudinal dispersion (m)	Alh	0-10
Transverse dispersion (m)	Ath	0.1*Alh
Diffusion coefficient (m^2/d)	Diffc	8.64e-5
Porosity (-)	Θ	0.35
Specific storitivity (-)	Ss	0.0001
Specific yield (-)	Sy	0.25
Injection concentration (mg/L)	C_inj	10
Ambient concentration (mg/L)	C_amb	1000
Cutoff (-)	CO	0.9
Injection/extraction volume (x10^3 m3)	V_inj/V_inj	10-100
Injection time	t_inj	90
Storage time (d)	t_storage	90
Extraction time (d)	t_ext	90
Ambient flow (m/y)	V_amb	0-100
Inner/outer iterations	N_inner/N_outer	9000

Appendix B

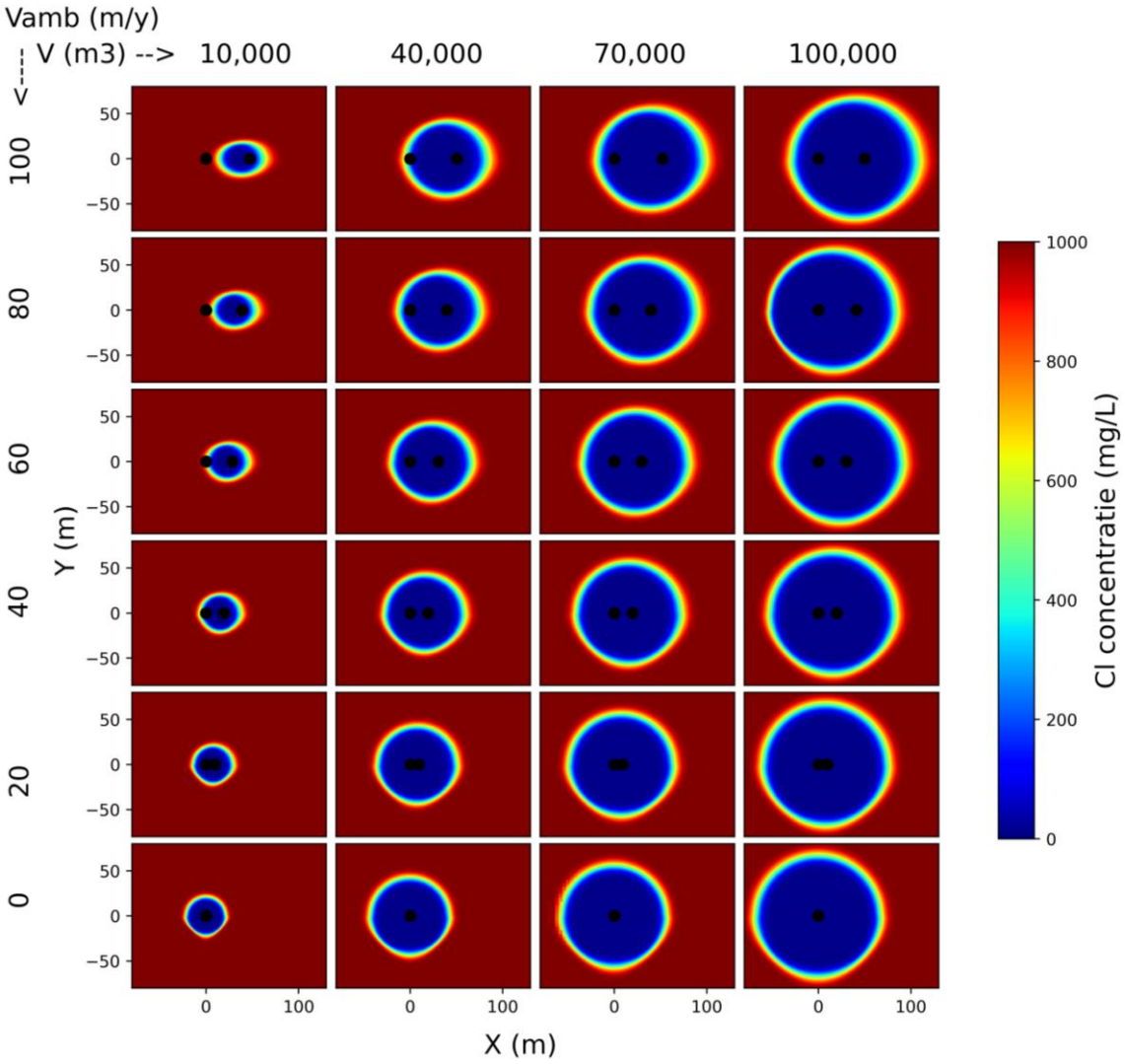

Figure 42. Shapes of all injection volumes from the base scenario at the start of extraction.